Shell finite elements with arbitrary displacement fields along the thickness

International Journal of Solids and Structures 321 (2025) 113544

Contents lists available at ScienceDirect

International Journal of Solids and Structures

journal homepage: www.elsevier.com/locate/ijsolstr

Shell finite elements with arbitrary displacement fields along the thickness

D. Scano [a,*,1], E. Carrera [a,b,2], E. Zappino [a,3]

[a] MUL² Lab, Department of Mechanical and Aerospace Engineering, Politecnico di Torino, Corso Duca degli Abruzzi 24, 10129 Torino, Italy
[b] Department of Mechanical Engineering, College of Engineering, Prince Mohammad Bin Fahd University, P.O. Box 1664, Al Khobar 31952, Kingdom of Saudi Arabia

ARTICLE INFO

Keywords:
Finite element method
Shell models
Carrera Unified Formulation
Refined theories
Taylor polynomials

ABSTRACT

This paper introduces an innovative approach for developing shell structural theories with an arbitrary kinematic field. In this study, each displacement component may be analysed using an independent expansion function. This method allows for the incorporation of both classical and higher-order theories within a unified framework. The Carrera Unified Formulation is employed to describe the thickness kinematics. In this paper, the structural theories are built by using polynomial terms. The finite element method is employed to discretize the structure in the reference mid-surface of the structure, utilizing Lagrange-based elements. The governing equations for the linear analysis are derived using the principle of virtual displacements. Also, the Mixed Interpolation of Tensorial Components is adopted inside the formulation to limit the locking issues. Cylindrical and spherical shells are studied here. Several radius-to-thickness ratios are taken into account. Both point and distributed loads are considered. Whenever possible, the present results are compared with the existing literature. The accuracy of the models presented is assessed for both displacements and stress outputs. The results illustrate that the selection of the most appropriate model is highly contingent on the specific parameters of the particular problem.

1. Introduction

Shell structures play a vital role in various engineering applications due to their efficient load-carrying capacities. In modern advanced engineering, which spans from industrial applications to biomechanics, complex and computationally intensive structural analyses are often necessary. To mitigate computational demands, appropriate two-dimensional (2D) shell models can be utilized to analyse three-dimensional (3D) continua, particularly for certain geometries. The shell models remain prevalent despite the improvements in computing power. These models are extensively applied in engineering, studying aircraft panels and cylindrical structures in the aerospace field, among others.

The thickness-wise deformation of shells. Structures typically experience deformation as a result of a variety of factors, including the types of loads, materials used, boundary conditions, geometrical properties, and other parameters that may arise in particular situations (Zappino and Carrera, 2018). The deformation pattern is a localized property contingent upon the particular problem being examined, representing a thickness-wise characteristic of the structure. Fig. 1 illustrates a shell subjected to point load and a localized pressure, where two edges are simply-supported. Specifically, three thickness-lines are considered, each exhibiting distinct behaviour in the deformed equilibrium state. Thickness-lines A and B are significantly influenced by the pressure, whereas the Thickness-line C undergoes minimal deformation. That is *it would not make sense to use the same degree of freedom for the three different thickness-lines.*

Classical and Refined shell approaches. During the centuries, numerous shell models have been presented. First, the Thin Shell Theory (TST) is considered the classical model. TST is founded upon Kirchhoff's hypotheses (Kirchhoff, 1850), which assume the absence of transverse shear and through-the-thickness deformation, thereby preserving the orthogonality of lines to the shell reference surface during deformation. The inclusion of transverse shear deformation leads to the Reissner–Mindlin theory (Reissner, 1945; Mindlin, 1951), commonly referred to as the First-Order Shear Deformation Theory (FSDT). For further insights, Naghdi's review (Naghdi, 1956) provides an overview of several classical theories. While classical theories are primarily suitable for isotropic and thin cases, they were widely utilized in the early development of Finite Element Method (FEM) shell formulations, as illustrated

* Corresponding author.
E-mail addresses: daniele.scano@polito.it (D. Scano), erasmo.carrera@polito.it (E. Carrera), enrico.zappino@polito.it (E. Zappino).
[1] PhD Student.
[2] Professor of Aeronautics and Astronautics.
[3] Associate Professor.

https://doi.org/10.1016/j.ijsolstr.2025.113544
Received 15 January 2025; Received in revised form 27 May 2025; Accepted 24 June 2025
Available online 9 July 2025

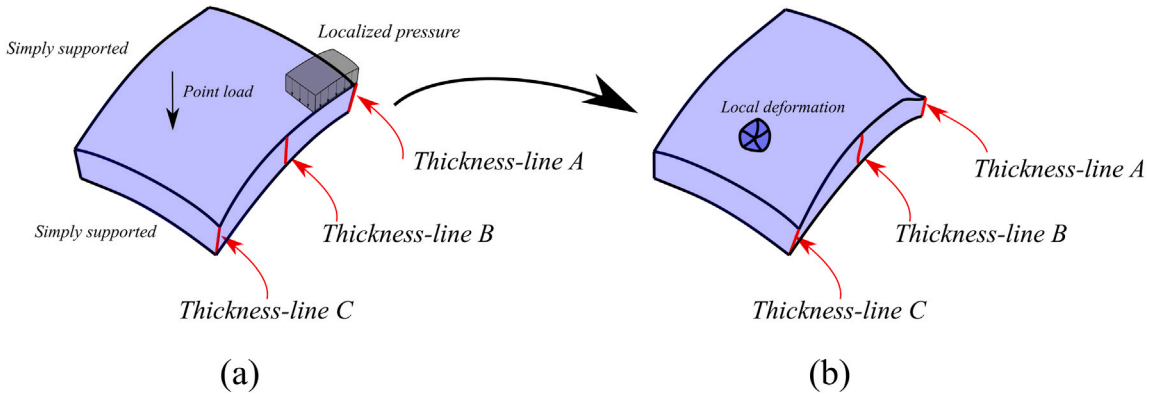

Fig. 1. Deformations localized across different thickness-lines of a shell structure: initial (a) and deformed (b) configurations.

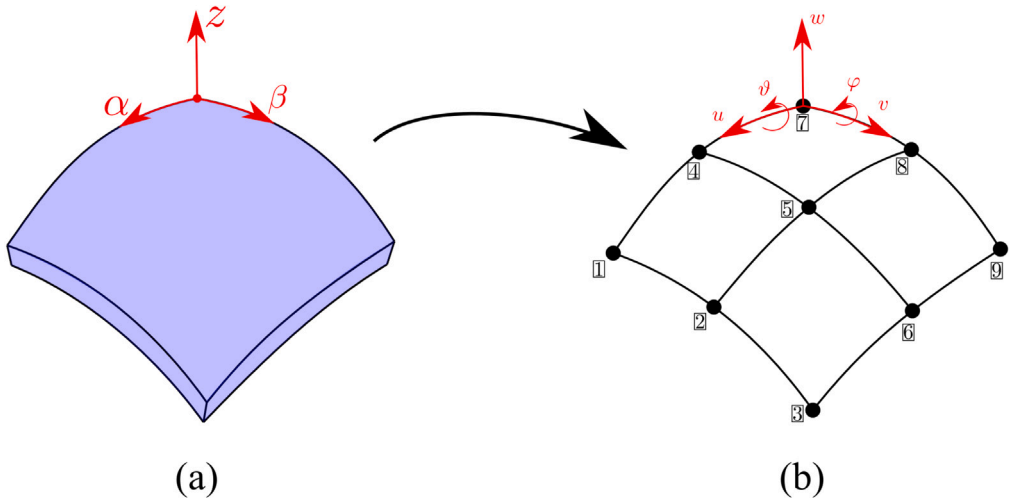

Fig. 2. Classical two-dimensional shell finite elements: real structure (a) and FE mesh (b).

by the work of Argyris (Argyris, 1966). Many shell elements are based on Lagrange polynomials; for example, Pryor and Barker (Pryor and Baeker, 1971) introduced a four-node element specifically to explore transverse shear effects. Classical models persist in contemporary commercial codes, with many still relying on them. Illustrating this, Fig. 2 depicts a shell structure discretized using classical four-node 2D elements. Each Finite Element (FE) node has three displacements and two rotations (3U+2R) as unknowns, resulting in only five Degrees Of Freedom (DOF) per node. More refined models use the rotation around the z axis. A comprehensive explanation of several classical FE may be found in Bathe (1996).

However, classical shell elements encounter several limitations when local effects and nonlinear deformations must be considered. In this way, 3D elements may be adopted to obtain more accurate results, even though the computational costs increase, as anticipated before. For more information, see the works of Argyris (1965) and Cinefra (2022). In 3D formulations, each FE node is specifically represented by only three displacements (3U). Fig. 3 illustrates a shell-like structure subdivided by a solid mesh. In this specific case, 8 nodes are used for each element. It is also possible to use 3D and 2D FE in the same numerical model, as shown by Surana (1980, 1982) and Dávila (1994). For a complete overview of the so-called *global/local* methods, please see the paper of Noor (1986). For example, Blanco et al. (2008) coupled incompatible 3D and 2D models under the Naghdi hypothesis. Liao et al. (1988) explored the connection between solid and shell FE for the non-linear analysis. Cofer and Will (Cofer and Will, 1991) proposed a transition element which is free from spurious zero energy modes. Recently, Zappino and Carrera (2018) introduced a

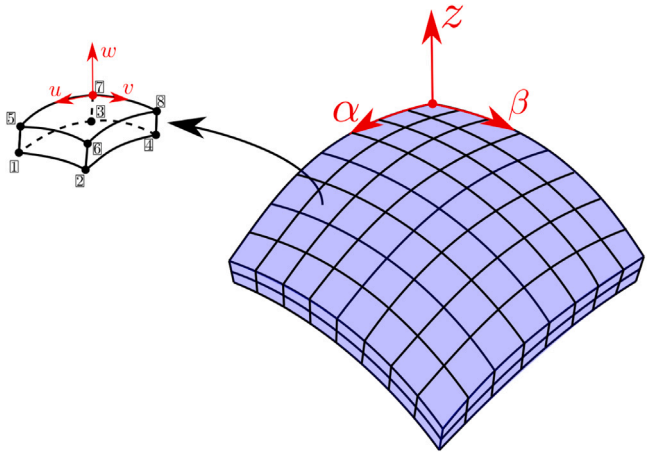

Fig. 3. Employing three-dimensional finite elements for discretizing a shell-like structure.

unified approach to incorporate 1D, 2D, and 3D models. The different types of elements may be connected in a consistent way without using mathematical artifices. This integration aims to reduce computational costs and enhance efficiency. In Fig. 4, a reinforced shell is depicted. In this case, it is convenient to discretize the cylindrical panel by using 2D elements, while the stiffeners are represented by a 3D mesh.

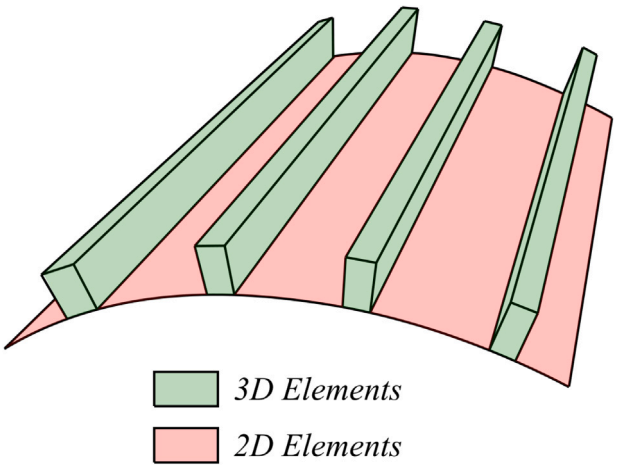

Fig. 4. Utilizing a global–local method for discretizing a structure, employing a combination of 3D and 2D mixed elements.

Several refined shell models have emerged over the last few decades. Firstly, axiomatic theories are briefly reviewed, where scientists have made assumptions regarding the behaviour of structures. For more details, significant insights can be found in the notable books by Reddy (1997) and Palazotto and Dennis (1992). Additionally, comprehensive reviews of advanced shell models are available in the works of Noor and Burton (1990) and Carrera (2001). Washizu (1968) provided more information regarding a general theory based on polynomial terms. Thus, the following displacement field may be written:

$$\begin{aligned} u_\alpha &= u_{\alpha_1} + z u_{\alpha_2} + z^2 u_{\alpha_3} + \cdots + z^{N-1} u_{\alpha_N} \\ u_\beta &= u_{\beta_1} + z u_{\beta_2} + z^2 u_{\beta_3} + \cdots + z^{N-1} u_{\beta_N} \\ u_z &= u_{z_1} + x u_{z_2} + z^2 u_{z_3} + \cdots + z^{N-1} u_{z_N} \end{aligned} \tag{1}$$

For instance, Reddy and Liu (1985) employed refined models to account for the parabolic distribution of the transverse shear stresses in the static and dynamic analyses of shell structures. Bhimaraddi (1984) studied free vibrations of circular cylindrical shells by incorporating higher-order terms for in-plane displacements. These models consider a constant transverse displacement as in the classical theories, neglecting the thickness stretching. Other scientists, however, have proposed models with parabolic approximations of the transverse component of the displacement field. For instance, refer to Hildebrand et al. (1940) and Khare et al. (2004).

The Carrera Unified Formulation vs axiomatic and asymptotic approaches. Finally, Carrera (1999a,b) proposed the so-called Carrera Unified Formulation (CUF). This method allows for the independent selection of the structural theory and shape functions over the mid-surface of the shell. CUF was employed for numerous applications. For example, Cinefra et al. (2016) investigated various benchmarks for thermal applications, while Carrera et al. (2018) studied multilayered sandwich shells embedding piezo-layers. Interested readers can find more details and references in Carrera (2003). Also, nonlinear cases have been considered in this context by Wu et al. (2021). Regarding the shape functions, the CUF literature presents a variety of elements, spanning from classical four-node to higher-order nine- and sixteen-node Lagrange-based elements. Additionally, hierarchical finite elements have been evaluated. See Pagani et al. (2023) for a comparison of the shape functions.

Another method to build shell models is based on the asymptotic approaches, where the 3D governing equations are expanded in terms of a perturbation parameter δ (typically the ratio of shell thickness to radius, e.g., $\delta = h/R$) from which theories corresponding to the same order in δ are derived. See the relevant book of Gol'denveizer (1961) for more information. One advantage of the asymptotic approach is its provision of "consistent" approximations, wherein all terms with a magnitude similar to the introduced perturbation parameter δ are retained in a given asymptotic theory. Additionally, as δ approaches zero, the method converges towards 3D solutions. However, as thickness increases, the convergence rate is expected to decrease. Despite this, the approach provides a straightforward estimation of solution accuracy compared to exact 3D solutions. Interesting results and conclusions are shown in the works of Cicala (1959, 1965). Furthermore, Yu et al. (2002) studied the bending behaviour of multilayered shells. Lee and Hodges (2009) presented a FE theory for the dynamic analysis of shells. Finally, Berdichevsky (2010) proposed an asymptotic method for studying sandwich shells.

Table 1
Complete fourth-order Taylor theory, number of terms = 15.

Variable	1	z	z^2	z^3	z^4
u_α	●	●	●	●	●
u_β	●	●	●	●	●
u_z	●	●	●	●	●

Table 2
Reduced fourth-order Taylor theory, number of terms = 10.

Variable	1	z	z^2	z^3	z^4
u_α	●	○	●	○	●
u_β	○	○	●	●	●
u_z	●	●	○	●	●

Aim of the present paper. The objective of this study is to develop a method for assessing the influence of each polynomial term within the expansion. The ultimate aim is to construct the most beneficial models, specifically reduced theories while maintaining the desired level of accuracy. To achieve this goal, it is helpful to visualize the models as depicted in Table 1, where a complete fourth-order Taylor theory is presented. The black dots indicate the inclusion of the term. Conversely, when investigating reduced models, it is advantageous to represent disregarded terms with white dots, as illustrated in Table 2. To explain this point better, consider again the example in Fig. 1. Each thickness-line of the structure could be effectively studied by a tailored model to accurately capture its thickness-wise deformation behaviour. See Fig. 5. As evident, for the analysis of Thickness-line B, the most detailed model with nine terms could be efficiently utilized. However, when considering Thickness-line A, the significance of higher-order terms for transverse displacement becomes apparent, particularly due to significant alterations in thickness in the deformed configuration.

Recently, a method to investigate the role of each term changing multiple parameters (e.g., radius-to-thickness ratios) has been presented (Carrera and Petrolo, 2010b; Petrolo and Carrera, 2019), termed as the Asymptotic–Axiomatic Method (AAM). This approach comprises several steps: (a) Selection of problem data; (b) Determination of the output variable; (c) Selection of a theory, wherein the terms considered for displacement variables are established; (d) Fixing a starting complete theory, often chosen as the reference model due to its provision of a 3D-like solution; (e) Derivation of governing equations by using a convenient framework as the CUF; (f) Calculation of the accuracy of the theory relative to the reference solution.

Using the AAM method, a two-dimensional plot can be generated, as depicted in Fig. 6(a). The error relative to the reference solution is shown on the horizontal axis, while the number of considered terms is indicated on the vertical axis. The error can be defined in several ways; typically, a relative error is employed. Various parameters can serve as the basis for error evaluation, such as displacements, stresses, or natural frequencies in dynamic analyses. It is important to note that this graph exhibits two significant properties: (a) it is dependent on the specific problem at hand, and (b) it varies based on the desired output. Four models are explicitly represented in the plot. Additionally, it is

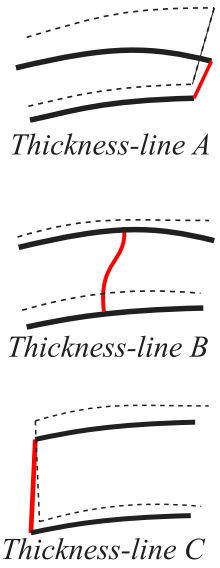

Variable	1	z	z^2	z^3	z^4
u_α	●	●	○	○	○
u_β	●	●	○	○	○
u_z	●	○	●	●	○

Variable	1	z	z^2	z^3	z^4
u_α	●	●	●	○	●
u_β	●	●	○	○	●
u_z	●	●	○	○	○

Variable	1	z	z^2	z^3	z^4
u_α	●	●	○	○	○
u_β	●	●	○	○	○
u_z	●	●	○	○	○

Fig. 5. Use of different reduced models for the study of three thickness-lines from Fig. 1.

evident how a displacement variable, such as u_α, may be completely disregarded in certain cases. This method facilitates the construction of the Best Theory Diagram (BTD), which represents the curve identifying all models with the least error for a given number of terms (Pareto Front). See Fig. 6(b). In this particular example, a complete fourth-order model (TE4) is utilized as the reference solution. When the number of terms falls below three, the problem can no longer be considered a general shell problem. This typically occurs in simplified cases, such as cylindrical bending. Additionally, the uniform complete theories are depicted. Moreover, literature models such as the Thin Shell Theory (TST) (Kirchhoff, 1850), First-order Shear Deformation Theory (FSDT) (Reissner, 1945; Mindlin, 1951), Reissner (Reissner, 1975), and Hildebrand, Reissner, and Thomas (HRT) (Hildebrand et al., 1940) may also be included in the same graph.

To the best of the authors' knowledge, a unified method for the automatic generation of reduced shell models in a unified framework, such as those illustrated in Table 2, has not been established. Preliminary works have been presented by Carrera et al. (2024b, 2025) for the beam and plate formulations. Carrera and co-authors (Petrolo et al., 2016; Carrera et al., 2011; Carrera and Petrolo, 2010a; Petrolo and Lamberti, 2016; Petrolo and Carrera, 2019) have explored the elimination of specific terms through a penalization technique. However, the stiffness matrix consistently retains the dimension of the starting accurate theory. For example, referring back to Table 1, all analyses maintain 15 terms for each FE node from a computational standpoint. Specifically, the efficacy of terms in Taylor-based expansions has been investigated within plate and shell formulations, encompassing displacement, stresses, and frequencies in dynamic responses. Another proposal for selecting different models for each displacement component was given by Demasi (2008), wherein the Generalized Unified Formulation (GUF) was introduced. A closed-form solution was presented for the analysis of plate structures. The GUF was also included in the FE framework (Demasi, 2013).

Proposal for determining the best computational model. This paper marks the initial stride toward systematically determining the most suitable theories for shell formulation. Subsequent works outlining further steps will be presented in the future. These steps can be summarized as follows:

1. The present paper establishes the theoretical foundations for creating reduced models. Currently, identical models are utilized for every point of the mid-surface;
2. A method for thickness-wise analysis of the shell is utilized, where each thickness-line is approximated using a distinct structural theory. For example, the Node Dependent Kinematics (NDK) method can be implemented leveraging the capabilities of the Carrera Unified Formulation (CUF) (Carrera et al., 2024a);
3. Analysing and classifying the proposed theories can be achieved through the implementation of the AAM;
4. Innovative techniques such as data mining and machine learning could be leveraged to analyse this information and reduce analysis time;
5. The ultimate aspiration is to develop a tool capable of determining the optimal model for a given level of accuracy while considering various factors such as boundary conditions, loadings, materials, and other pertinent characteristics.

The previous steps will be integrated into a single procedure by employing the possibilities of CUF. In Carrera et al. (2024b, 2025), detailed explanations of the method are given.

Also, the method have several advantages over the solid shell formulations. First, solid shell formulations are affected by issues related to aspect ratio. In the solid shell approach, elements typically use bilinear shape functions on the mid-surface, while the thickness direction is discretized using a linear model (see Fig. 3). This configuration enables the analysis of higher-order effects by employing multiple elements through the thickness. However, to avoid excessive element distortion, additional elements must also be introduced in the in-plane directions. In shell formulations, the finite element discretization is decoupled from the underlying structural theory, allowing the adoption of higher-order models without modifying the mesh. Also, solid shell formulations face challenges when modelling very thin structures due to numerical difficulties and mesh quality concerns. Finally, the present method permits the choice of the desired structural theories without any restraints and maintains the same finite element mesh. This provides both flexibility and efficiency in the analysis of complex structures.

Contents of this work. In this paper, the CUF is able to use models based on polynomial terms, similar to that exemplified in Table 2. For this purpose, the assembly of the arrays of the FE models in the unified formulation had to be redefined. A scalar Fundamental Nucleus (FN) serves as the kernel for defining the global stiffness matrix, eliminating the need for excluding terms via penalization techniques. The current assembly method facilitates the derivation of a stiffness matrix with uniform dimensions. Specifically, the effective dimension of the stiffness matrix (as well as the unknown and load vectors) depends on the kinematic model. Ultimately, this introductory paper concentrates on analysing isotropic structures, covering a range from compact to thin-walled shells. Subsequent research will delve into exploring the AAM methodology.

Finally, it is important to highlight that FE analysis can face significant stiffening challenges when dealing with thin structures. Shell elements are particularly susceptible to shear and membrane locking issues. Shear locking occurs when finite elements are unable to accurately calculate bending deformation, resulting in the erroneous absorption of strain energy by shear modes. As structures become thinner, transverse shear energy tends towards zero. Meanwhile, membrane locking arises when mid-surface stretching during bending deformation is inaccurately computed, leading to membrane energy dominance over bending energy. Addressing these issues, the Mixed Interpolation of Tensorial Components (MITC) method (Bathe and Dvorkin, 1986; Bucalem and Bathe, 1993) has been proposed to mitigate FE locking phenomena. In the unified formulation context, Cinefra and Carrera (2013) introduced a nine-node Lagrange-based element incorporating this integration scheme.

This paper is organized in the following way: (a) Section 2 reviews various shell theories from the literature, accompanied by illustrations of Taylor-based expansions and an explanation of reduced theories. (b)

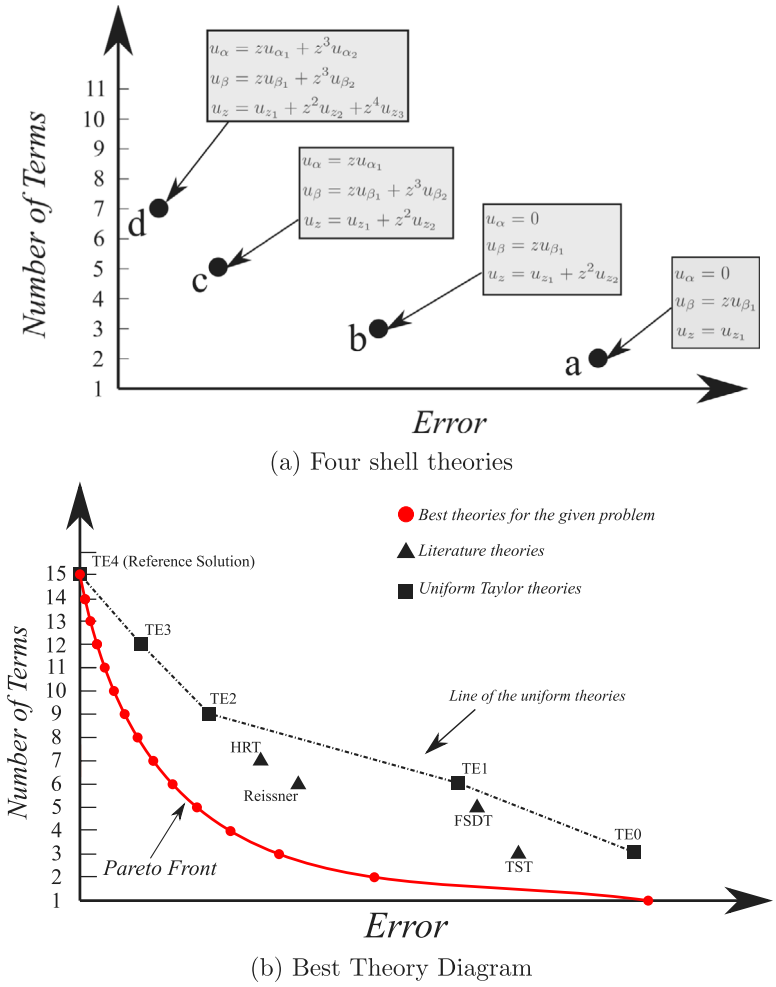

Fig. 6. Representation of in a 2D plot Error-Number of Terms (a) and example of a Best Theory Diagram (b).

Section 3 outlines the basis of the Unified formulation approximation and how it is integrated into the finite element method. (c) In Section 4, the governing equations are derived by adopting the principle of virtual displacements. (d) To illustrate the new method, Section 5 shows an exhaustive example for the assembly of the arrays. (e) Section 6 showcases results pertaining to displacements and stresses. (f) Section 7 draws the main conclusions and illustrates the possible forthcoming advances.

2. Review of the shell theories

Consider a generic isotropic shell structure depicted in Fig. 7, described by curvilinear reference system (α, β, z). In the shell structures, two radii of curvatures have to be taken into account, namely R_α and R_β. In particular, thickness-line A is oriented along the thickness direction z. Therefore, the mid-surface Ω lies in the $\alpha - \beta$ plane of the structure. The three-dimensional displacement field is generally described as:

$$\mathbf{u}(\alpha,\beta,z) = \left\{ \begin{array}{ccc} u_\alpha(\alpha,\beta,z), & u_\beta(\alpha,\beta,z), & u_z(\alpha,\beta,z) \end{array} \right\}^T \tag{2}$$

In the Introduction section, several models have been mentioned without providing their explicit expressions. In this section, the mathematical assumptions underlying the classical theories are presented. Furthermore, a detailed explanation of some of the most well-known refined theories is provided. This approach facilitates a natural progression towards the choice of Taylor polynomials. Additionally, these models are presented in alignment with the reference system depicted in Fig. 7.

2.1. Classical shell theories

The first theory is the Thin Shell Theory (TST) (Kirchhoff, 1850), and the displacement field can be written as follows:

$$\begin{array}{rcl} u_\alpha(\alpha,\beta,z) & = & u_{\alpha_1}(\alpha,\beta) - \frac{\partial u_{z_1}(\alpha,\beta)}{\partial \alpha} z \\ u_\beta(\alpha,\beta,z) & = & u_{\beta_1}(\alpha,\beta) - \frac{\partial u_{z_1}(\alpha,\beta)}{\partial \beta} z \\ u_z(\alpha,\beta,z) & = & u_{z_1}(\alpha,\beta) \end{array} \tag{3}$$

Second, the displacement field of the First-order Shear Deformation Theory (FSDT) (Reissner, 1945; Mindlin, 1951) is given in the following:

$$\begin{array}{rcl} u_\alpha(\alpha,\beta,z) & = & u_{\alpha_1}(\alpha,\beta) + \phi_\beta(\alpha,\beta) z \\ u_\beta(\alpha,\beta,z) & = & u_{\beta_1}(\alpha,\beta) + \phi_\alpha(\alpha,\beta) z \\ u_z(\alpha,\beta,z) & = & u_{z_1}(\alpha,\beta) \end{array} \tag{4}$$

In this notation, u_{α_1}, u_{β_1}, and u_{z_1} represent the displacements of the reference mid-surface of the shell, while ϕ_β and ϕ_α denote the rotations around the β and α axes, respectively. Additionally, $-\frac{\partial u_{z_1}(\alpha,\beta)}{\partial \alpha}$ and $-\frac{\partial u_{z_1}(\alpha,\beta)}{\partial \beta}$ describe the rotations around the β and α axes when the shear deformation is neglected. The classical theories are shown in Fig. 8 in the $\alpha - z$ and $\beta - z$ planes for completeness.

2.2. Use of ad-hoc higher-order theories

As anticipated, refined theories have been proposed to accurately describe the stresses and evaluate the displacements when the structures are thicker and/or subjected to particular loading conditions. One

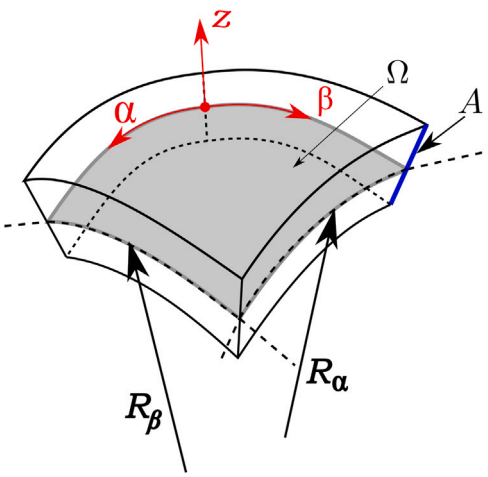

Fig. 7. Reference system for a generic shell-like structure.

of the first models was presented by Hildebrand, Reissner, and Thomas (HRT) (Hildebrand et al., 1940), where the u_z variable contains first- and second-order terms:

$$\begin{aligned} u_\alpha &= u_{\alpha_1} + z u_{\alpha_2} \\ u_\beta &= u_{\beta_1} + z u_{\beta_2} \\ u_z &= u_{z_1} + z u_{z_2} + z^2 u_{z_3} \end{aligned} \tag{5}$$

On the contrary, other scientists focussed on the development of theories where the higher-order terms are present only for the in-plane displacements u_α and u_β. For instance, the following model was used by Thakur et al. (2018):

$$\begin{aligned} u_\alpha &= u_{\alpha_1} + z u_{\alpha_2} + z^2 u_{\alpha_3} + z^3 u_{\alpha_4} \\ u_\beta &= u_{\beta_1} + z u_{\beta_2} + z^2 u_{\beta_3} + z^3 u_{\beta_4} \\ u_z &= u_{z_1} \end{aligned} \tag{6}$$

Finally, it is surely possible to adopt a higher-order theory for all three displacements. Khare et al. (2004) proposed the following field:

$$\begin{aligned} u_\alpha &= u_{\alpha_1} + z u_{\alpha_2} + z^2 u_{\alpha_3} + z^3 u_{\alpha_4} \\ u_\beta &= u_{\beta_1} + z u_{\beta_2} + z^2 u_{\beta_3} + z^3 u_{\beta_4} \\ u_z &= u_{z_1} + z u_{z_2} + z^2 u_{z_3} \end{aligned} \tag{7}$$

The previous equations provide excellent examples of how researchers can tailor shell models to analyse several problems while reducing the degrees of freedom efficiently. These concepts will be further explained in the upcoming Section 2.3, where Taylor-based models will be introduced.

2.3. Taylor-based higher-order theories

After describing the classical and literature models, the one-dimensional Taylor polynomials can be used to create structural theories to analyse the shell thickness-lines. The terms of these polynomials have the form z^b, where b denotes a positive integer. Carrera and co-workers (Carrera, 2003; Petrolo and Carrera, 2019) used these polynomials in many works. Usually, terms up to the fourth order are adopted, even though more refined theories have been used to analyse complicated phenomena (Petrolo et al., 2023).

Uniform theories. First, the *uniform* theories are presented. In these cases, all three displacement variables use the same complete expansion. In the previous works of the CUF literature, these models are extensively adopted and explained. A complete fifth-order model is shown below:

$$\begin{aligned} u_\alpha &= u_{\alpha_1} + z u_{\alpha_2} + z^2 u_{\alpha_3} + z^3 u_{\alpha_4} + z^4 u_{\alpha_5} + z^5 u_{\alpha_6} \\ u_\beta &= u_{\beta_1} + z u_{\beta_2} + z^2 u_{\beta_3} + z^3 u_{\beta_4} + z^4 u_{\beta_5} + z^5 u_{\beta_6} \\ u_z &= u_{z_1} + z u_{z_2} + z^2 u_{z_3} + z^3 u_{z_4} + z^4 u_{z_5} + z^5 u_{z_6} \end{aligned} \tag{8}$$

Different theories. It is also possible to use *different* theories for each displacement variable. In the previous Section 2.2, the three models approximated u_α and u_β with the same expansion, but it is more convenient to adopt dissimilar models in some problems, as shown below:

$$\begin{aligned} u_\alpha &= u_{\alpha_1} + z u_{\alpha_2} \\ u_\beta &= u_{\beta_1} + z u_{\beta_2} + z^2 u_{\beta_3} + z^3 u_{\beta_4} + z^4 u_{\beta_5} + z^5 u_{\beta_6} \\ u_z &= u_{z_1} + z u_{z_2} + z^2 u_{z_3} \end{aligned} \tag{9}$$

In the previous set, a first-order expansion for u_α is adopted, u_β uses a complete fifth-order expansion, and u_z is described by a parabolic model. The total number of terms is eleven, while Eq. (8) has eighteen terms.

Reduced theories. The next step is to create theories where the scientists have the possibility to freely decide the presence of the single terms. That is, the *reduced* theories may be derived. In fact, it could be more efficient to discard some parts from the complete expansions for specific cases. Thus, the following is given as an example:

$$\begin{aligned} u_\alpha &= u_{\alpha_1} + z^2 u_{\alpha_2} \\ u_\beta &= u_{\beta_1} + z u_{\beta_2} + z^3 u_{\beta_3} + z^5 u_{\beta_4} \\ u_z &= u_{z_1} \end{aligned} \tag{10}$$

In this model, only seven terms are present, while Eq. (8) uses eighteen ones. Please note that the subscripts are adjusted. It is interesting to note how u_α is a second-order term, but the linear term is disregarded. This example shows that the scholars are not restrained in deciding the most suitable model to be used.

In the CUF literature, the elimination of a term is accomplished through a penalization technique, which begins with a complete uniform theory. As a result, the effective number of terms (and, therefore, the computational cost) remains constant. For a more comprehensive explanation, please refer to Carrera et al. (2014).

3. Unified formulation for shell and generalization to the higher-order theories

After describing the possible models that can be used to describe shell structures, it would be beneficial to have a method to incorporate all these theories into a single framework. Thus, the Unified Formulation was proposed. In this approach, a 3D problem can be reduced to a 2D one, where a generic variable f is expressed in terms of M additional variables $f_\tau (\tau = 1, \dots, M)$. This expansion is constructed by introducing the base functions $F_\tau(z)$, which are defined along the shell thickness-line, as expressed below:

$$f(\alpha, \beta, z) = \sum_{\tau=1}^{M} F_\tau(z) f_\tau(\alpha, \beta) = F_\tau(z) f_\tau(\alpha, \beta), \qquad \tau = 1, 2, \dots, M \tag{11}$$

In this formulation, the Einstein summation convention is adopted. It is worth noting that a polynomial term z^b corresponds to an expansion function F_τ. While displacement components are used in this work, other choices, such as stress or strain components, can also be considered, as discussed in Carrera (2001).

In this manner, the 3D displacement field can be represented by a general expansion. Specifically, each displacement component is

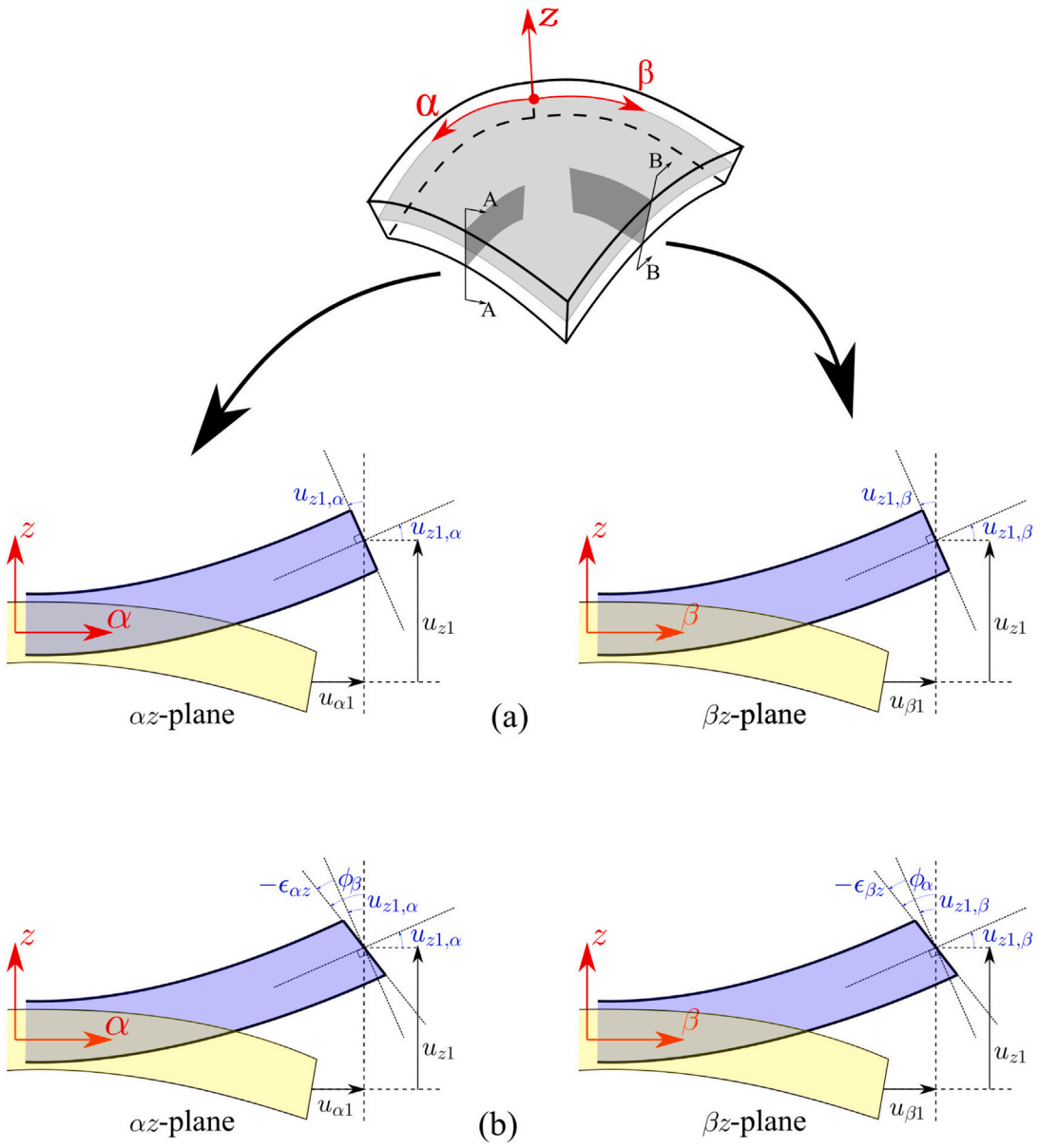

Fig. 8. Differences between classical shell theories: Thin Shell Theory (TST) (a) and First-order Shear Deformation Theory (FSDT).

described by different base functions as written below:

$$\begin{aligned} u_\alpha &= F_{u_\alpha \tau}(z) u_{\alpha_\tau}(\alpha,\beta) \quad \text{with} \quad \tau = 1,\dots,M_{u_\alpha} \\ u_\beta &= F_{u_\beta \tau}(z) u_{\beta_\tau}(\alpha,\beta) \quad \text{with} \quad \tau = 1,\dots,M_{u_\beta} \\ u_z &= F_{u_z \tau}(z) u_{z_\tau}(\alpha,\beta) \quad \text{with} \quad \tau = 1,\dots,M_{u_z} \end{aligned} \tag{12}$$

where $F_{u_\alpha \tau}$, $F_{u_\beta \tau}$, and $F_{u_z \tau}$ denote the expansion functions for the generalized displacements u_{α_τ}, u_{β_τ}, and u_{z_τ}. In previous CUF-based works (Carrera, 2003; Carrera et al., 2014), the expansions were simply denoted as F_τ since all three displacement components utilized the same model. Furthermore, M_{u_α}, M_{u_β}, and M_{u_z} indicate the number of expansions for each displacement variables.

If the principle of virtual displacements is adopted to derive the governing equations, then the virtual variations of the displacement field are given in the following:

$$\begin{aligned} u_\alpha &= F_{u_\alpha s}(z) \delta u_{\alpha_s}(\alpha,\beta) \quad \text{with} \quad s = 1,\dots,M_{u_\alpha} \\ u_\beta &= F_{u_\beta s}(z) \delta u_{\beta_s}(\alpha,\beta) \quad \text{with} \quad s = 1,\dots,M_{u_\beta}. \\ u_z &= F_{u_z s}(z) \delta u_{z_s}(\alpha,\beta) \quad \text{with} \quad s = 1,\dots,M_{u_z} \end{aligned} \tag{13}$$

where δ stands for the virtual variations. $F_{u_\alpha s}$, $F_{u_\beta s}$, and $F_{u_z s}$ are the expansion functions in the virtual system. As can be noted, the subscript τ is replaced by s.

In this work, however, the Finite Element Method (FEM) is used in union with the CUF to obtain numerical results and study structures without geometrical restraints. FEM approximates the unknowns over the shell mid-plane. Thus, the displacements can be expressed as shown

below:

$$u_\alpha = N_i(\alpha,\beta)F_{u_\alpha\tau}(z)q_{\alpha_{\tau i}} \quad \text{with} \quad \tau = 1,\dots,M_{u_\alpha} \quad \text{and} \quad i = 1,\dots,N_n$$
$$u_\beta = N_i(\alpha,\beta)F_{u_\beta\tau}(z)q_{\beta_{\tau i}} \quad \text{with} \quad \tau = 1,\dots,M_{u_\beta} \quad \text{and} \quad i = 1,\dots,N_n. \tag{14}$$
$$u_z = N_i(\alpha,\beta)F_{u_z\tau}(z)q_{z_{\tau i}} \quad \text{with} \quad \tau = 1,\dots,M_{u_z} \quad \text{and} \quad i = 1,\dots,N_n$$

while their virtual variations are written as follows:

$$u_\alpha = N_j(\alpha,\beta)F_{u_\alpha s}(z)\delta q_{\alpha_{sj}} \quad \text{with} \quad s = 1,\dots,M_{u_\alpha} \quad \text{and} \quad j = 1,\dots,N_n$$
$$u_\beta = N_j(\alpha,\beta)F_{u_\beta s}(z)\delta q_{\beta_{sj}} \quad \text{with} \quad s = 1,\dots,M_{u_\beta} \quad \text{and} \quad j = 1,\dots,N_n. \tag{15}$$
$$u_z = N_j(\alpha,\beta)F_{u_z s}(z)\delta q_{z_{sj}} \quad \text{with} \quad s = 1,\dots,M_{u_z} \quad \text{and} \quad j = 1,\dots,N_n$$

N_i and N_j stands for the shape functions, the repeated subscripts i and j indicate summation, N_n is the number of the shape functions per element. The nine-node Lagrange-based element is used for all the analyses. See Bathe (1996) for more information.

For clarity and brevity, a compact notation can be introduced for the real and virtual systems as follows:

$$u_l = N_i F_{u_l\tau} q_{l_{\tau i}} = \sum_i^{N_n}\sum_\tau^{M_{u_l}} N_i F_{u_l\tau} q_{l_{\tau i}} \tag{16}$$

$$\delta u_m = N_j F_{u_m s}\delta q_{m_{sj}} = \sum_j^{N_n}\sum_s^{M_{u_m}} N_j F_{u_m s}\delta q_{m_{sj}} \tag{17}$$

In this formulation, there is no summation over l (or m). The terms l and m can take the values α, β, and z.

4. Governing equations and finite element matrices

The present Section outlines the steps to derive governing equations by using the assumptions shown previously.

First, according to the classical elasticity, stress, $\boldsymbol{\sigma}$, and strain, $\boldsymbol{\epsilon}$, tensors may be conveniently expressed in vectorial form as given below:

$$\boldsymbol{\sigma} = \left\{ \begin{array}{cccccc} \sigma_{\alpha\alpha} & \sigma_{\beta\beta} & \sigma_{zz} & \sigma_{\beta z} & \sigma_{\alpha z} & \sigma_{\alpha\beta} \end{array} \right\}^T$$
$$\boldsymbol{\epsilon} = \left\{ \begin{array}{cccccc} \epsilon_{\alpha\alpha} & \epsilon_{\beta\beta} & \epsilon_{zz} & \epsilon_{\beta z} & \epsilon_{\alpha z} & \epsilon_{\alpha\beta} \end{array} \right\}^T \tag{18}$$

Second, the geometrical relations between strains and displacements are defined as follows:

$$\boldsymbol{\epsilon} = \mathbf{D}\mathbf{u} \tag{19}$$

where $\mathbf{D}$ is the matrix of differential operators. If small displacements and angles of rotations are considered, the matrix $\mathbf{D}$ reads as:

$$\mathbf{D} = \begin{bmatrix} \frac{\partial_\alpha}{H_\alpha} & 0 & \frac{1}{H_\alpha R_\alpha} \\ 0 & \frac{\partial_\beta}{H_\beta} & \frac{1}{H_\beta R_\beta} \\ 0 & 0 & \partial_z \\ \partial_z - \frac{1}{H_\alpha R_\alpha} & 0 & \frac{\partial_\alpha}{H_\alpha} \\ 0 & \partial_z - \frac{1}{H_\beta R_\beta} & \frac{\partial_\beta}{H_\beta} \\ \frac{\partial_\beta}{H_\beta} & \frac{\partial_\alpha}{H_\alpha} & 0 \end{bmatrix} \tag{20}$$

where $\partial_\alpha = \frac{\partial(\cdot)}{\partial\alpha}$, $\partial_\beta = \frac{\partial(\cdot)}{\partial\beta}$, $\partial_z = \frac{\partial(\cdot)}{\partial z}$, $H_\alpha = 1 + \frac{z}{R_\alpha}$, and $H_\beta = 1 + \frac{z}{R_\beta}$.

Third, the constitutive relation between strains and stresses for a linear elastic isotropic material can be expressed below:

$$\boldsymbol{\sigma} = \mathbf{C}\boldsymbol{\epsilon} \tag{21}$$

where the matrix of material coefficients, $\mathbf{C}$, is the following:

$$\mathbf{C} = \begin{bmatrix} C_{11} & C_{12} & C_{13} & 0 & 0 & 0 \\ C_{12} & C_{22} & C_{23} & 0 & 0 & 0 \\ C_{13} & C_{32} & C_{33} & 0 & 0 & 0 \\ 0 & 0 & 0 & C_{55} & 0 & 0 \\ 0 & 0 & 0 & 0 & C_{44} & 0 \\ 0 & 0 & 0 & 0 & 0 & C_{66} \end{bmatrix} \tag{22}$$

For the sake of completeness, the stress components can be written in the followings

$$\begin{aligned} \sigma_{\alpha\alpha} &= C_{11}\epsilon_{\alpha\alpha} + C_{12}\epsilon_{\beta\beta} + C_{13}\epsilon_{zz} \\ \sigma_{\beta\beta} &= C_{12}\epsilon_{\alpha\alpha} + C_{22}\epsilon_{\beta\beta} + C_{23}\epsilon_{zz} \\ \sigma_{zz} &= C_{13}\epsilon_{\alpha\alpha} + C_{23}\epsilon_{\beta\beta} + C_{33}\epsilon_{zz} \\ \sigma_{\beta z} &= C_{44}\epsilon_{\beta z} \\ \sigma_{\alpha z} &= C_{55}\epsilon_{\alpha z} \\ \sigma_{\alpha\beta} &= C_{66}\epsilon_{\alpha\beta} \end{aligned} \tag{23}$$

4.1. MITC Q9

As previously mentioned, the Mixed Interpolation of Tensorial Components (MITC) method is employed to address the shear locking issue inherent in Finite Element (FE) formulations. This FE method is commonly referred to as MITC Q9. For further details, refer to Bucalem and Bathe (1993).

In this approach, instead of directly computing the strain components from the displacements, an interpolation of these components is conducted within each element. This entails employing a specific interpolation strategy tailored to each strain component. Notably, the transverse normal strain, ϵ_{zz}, is not involved in this procedure and is directly calculated from the displacements. Fig. 9 illustrates the positions of the tying points and their coordinates in the $\xi - \eta$ natural plane, where $\xi = [-1, +1]$ and $\eta = [-1, +1]$.

Lagrangian functions are selected as the interpolating functions and are organized into the following arrays:

$$\begin{aligned} N_{m1} &= \left[\begin{array}{cccccc} N_{A1} & N_{B1} & N_{C1} & N_{D1} & N_{E1} & N_{F1} \end{array} \right] \\ N_{m2} &= \left[\begin{array}{cccccc} N_{A2} & N_{B2} & N_{C2} & N_{D2} & N_{E2} & N_{F2} \end{array} \right] \\ N_{m3} &= \left[\begin{array}{cccc} N_P & N_Q & N_R & N_S \end{array} \right] \end{aligned} \tag{24}$$

From this point on, the subscripts $m1$, $m2$ and $m3$ denote quantities calculated in the points $(A1, B1, C1, D1, E1, F1)$, $(A2, B2, C2, D2, E2, F2)$ and (P, Q, R, S), respectively. Consequently, the strain components can be rewritten as follows:

$$\begin{aligned} \epsilon_{\alpha\alpha} &= \sum_{m1=1}^{6} N_{m1}\epsilon_{\alpha\alpha_{m1}} = N_{m1}\epsilon_{\alpha\alpha_{m1}} \\ \epsilon_{\beta\beta} &= \sum_{m2=1}^{6} N_{m2}\epsilon_{\beta\beta_{m2}} = N_{m2}\epsilon_{\beta\beta_{m2}} \\ \epsilon_{zz} &= \epsilon_{zz} \\ \epsilon_{\beta z} &= \sum_{m2=1}^{6} N_{m2}\epsilon_{\beta z_{m2}} = N_{m2}\epsilon_{\beta z_{m2}} \\ \epsilon_{\alpha z} &= \sum_{m1=1}^{6} N_{m1}\epsilon_{\alpha z_{m1}} = N_{m1}\epsilon_{\alpha z_{m1}} \\ \epsilon_{\alpha\beta} &= \sum_{m3=1}^{4} N_{m3}\epsilon_{\alpha\beta_{m3}} = N_{m3}\epsilon_{\alpha\beta_{m3}} \end{aligned} \tag{25}$$

In this equation, the strains $\epsilon_{\alpha\alpha_{m1}}$, $\epsilon_{yy_{m2}}$, $\epsilon_{\alpha\beta_{m3}}$, $\epsilon_{\alpha z_{m1}}$, and $\epsilon_{\beta z_{m2}}$ are obtained using Eq. (19), where the shape functions N_i are computed at the tying points.

For the sake of clarity, the strains can be extensively written with the CUF (Eq. (12)) and the FEM (Eq. (14)) approximations with the

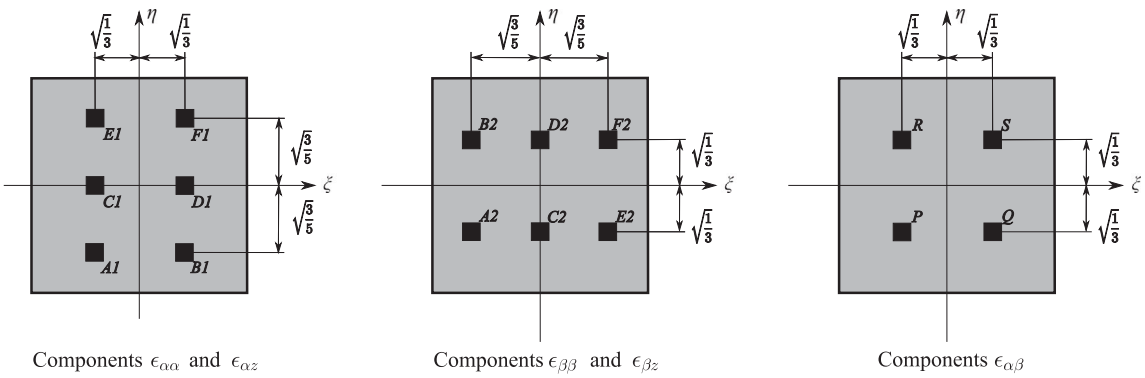

Fig. 9. Tying points for the MITC Q9 shell elements used for different strain components.

MITC method, as follows:

$$
\begin{aligned}
\epsilon_{\alpha\alpha} &= \frac{1}{H_\alpha} N_{m1} N^{m1}_{i,\alpha} F_{u_\alpha\tau} q_{\alpha_{\tau i}} + \frac{1}{H_\alpha R_\alpha} N_{m1} N^{m1}_{i} F_{u_z\tau} q_{z_{\tau i}} \\
\epsilon_{\beta\beta} &= \frac{1}{H_\beta} N_{m1} N^{m1}_{i,\beta} F_{u_\beta\tau} q_{\beta_{\tau i}} + \frac{1}{H_\beta R_\beta} N_{m1} N^{m1}_{i} F_{u_z\tau} q_{z_{\tau i}} \\
\epsilon_{zz} &= N_i F_{u_z\tau,z} q_{z_{\tau i}} \\
\epsilon_{\beta z} &= N_{m2} N^{m2}_{i} F_{u_{\beta\tau},z} q_{\beta_{\tau i}} - \frac{1}{H_\beta R_\beta} N_{m2} N^{m2}_{i} F_{u_{\beta\tau},z} q_{\beta_{\tau i}} + \frac{1}{H_\beta} N_{m2} N^{m2}_{i,\beta} F_{u_z\tau} q_{z_{\tau i}} \\
\epsilon_{\alpha z} &= N_{m1} N^{m1}_{i} F_{u_{\alpha\tau},z} q_{\alpha_{\tau i}} - \frac{1}{H_\alpha R_\alpha} N_{m1} N^{m1}_{i} F_{u_{\alpha\tau},z} q_{\alpha_{\tau i}} + \frac{1}{H_\alpha} N_{m1} N^{m1}_{i,\alpha} F_{u_z\tau} q_{z_{\tau i}} \\
\epsilon_{\alpha\beta} &= \frac{1}{H_\beta} N_{m3} N^{m3}_{j,\beta} F_{u_\alpha\tau} q_{\alpha_{\tau i}} + \frac{1}{H_\alpha} N_{m3} N^{m3}_{j,\alpha} F_{u_\beta\tau} q_{\beta_{\tau i}}
\end{aligned}
\tag{26}
$$

The virtual variations of the strains can be straightforwardly expressed by employing Eqs. (13) and (15). Here, the subscripts $m1$, $m2$, and $m3$ are replaced by $n1$, $n2$, and $n3$ respectively. The explicit expressions can be written in the following:

$$
\begin{aligned}
\delta\epsilon_{\alpha\alpha} &= \frac{1}{H_\alpha} N_{n1} N^{n1}_{j,\alpha} F_{u_\alpha s} \delta q_{\alpha_{sj}} + \frac{1}{H_\alpha R_\alpha} N_{n1} N^{n1}_{j} F_{u_z s} \delta q_{z_{sj}} \\
\delta\epsilon_{\beta\beta} &= \frac{1}{H_\beta} N_{n1} N^{n1}_{j,\beta} F_{u_\beta s} \delta q_{\beta_{sj}} + \frac{1}{H_\beta R_\beta} N_{n1} N^{n1}_{j} F_{u_z s} \delta q_{z_{sj}} \\
\delta\epsilon_{zz} &= N_j F_{u_z s,z} \delta q_{z_{\tau i}} \\
\delta\epsilon_{\beta z} &= N_{n2} N^{n2}_{j} F_{u_\beta s,z} \delta q_{\beta_{sj}} - \frac{1}{H_\beta R_\beta} N_{n2} N^{n2}_{j} F_{u_\beta s,z} \delta q_{\beta_{sj}} + \frac{1}{H_\beta} N_{n2} N^{n2}_{j,\beta} F_{u_z s} \delta q_{z_{sj}} \\
\delta\epsilon_{\alpha z} &= N_{n1} N^{n1}_{j} F_{u_\alpha s,z} \delta q_{\alpha_{sj}} - \frac{1}{H_\alpha R_\alpha} N_{n1} N^{n1}_{j} F_{u_\alpha s,z} \delta q_{\alpha_{sj}} + \frac{1}{H_\alpha} N_{n1} N^{n1}_{j,\alpha} F_{u_z s} \delta q_{z_{sj}} \\
\delta\epsilon_{\alpha\beta} &= \frac{1}{H_\beta} N_{n3} N^{n3}_{j,\beta} F_{u_\alpha s} \delta q_{\alpha_{sj}} + \frac{1}{H_\alpha} N_{n3} N^{n3}_{j,\alpha} F_{u_\beta s} \delta q_{\beta_{sj}}
\end{aligned}
\tag{27}
$$

4.2. Governing equations

If the principle of virtual work is employed

$$
\delta L_{int} = \delta L_{ext} \tag{28}
$$

First, the virtual internal work is taken into account and reads as:

$$
\begin{aligned}
\delta L_{int} &= \int_V \delta\boldsymbol{\epsilon}^T \boldsymbol{\sigma} H_\alpha H_\beta \mathrm{d}\alpha\mathrm{d}\beta\mathrm{d}z \\
&= \int_V \left(\delta\epsilon_{\alpha\alpha}\sigma_{\alpha\alpha} + \delta\epsilon_{\beta\beta}\sigma_{\beta\beta} + \delta\epsilon_{zz}\sigma_{zz} + \delta\epsilon_{\beta z}\sigma_{\beta z} + \delta\epsilon_{\alpha z}\sigma_{\alpha z} + \delta\epsilon_{\alpha\beta}\sigma_{\alpha\beta}\right) \\
&\quad \times H_\alpha H_\beta \mathrm{d}\alpha\mathrm{d}\beta\mathrm{d}z
\end{aligned}
\tag{29}
$$

In this paper, consistent with the CUF literature, the engineering shear strains are defined without the factor of '1/2'. As a result, the corresponding shear deformation terms do not require a factor of '2' in the formulation.

The expression for the internal work can be derived using the MITC method (Eqs. (26) and (27)), the CUF and the FEM approximations (Eqs. (14) and (15)), and the constitutive equations (Eq. (21)). For the sake of brevity, it is not displayed explicitly.

Second, the virtual external work due to the point loads can be written as:

$$
\delta L_{ext} = \delta\mathbf{u}^T \mathbf{P} = \left(\delta u_\alpha P_{u_\alpha} + \delta u_\beta P_{u_\beta} + \delta u_z P_{u_z}\right) \tag{30}
$$

Then, the CUF and FEM (Eq. (15)) approximations can be inserted to obtain:

$$
\delta L_{ext} = \delta q_{\alpha_{sj}} N_j F_{u_\alpha s} P_{u_\alpha} + \delta q_{\beta_{sj}} N_j F_{u_\beta s} P_{u_\beta} + \delta q_{z_{sj}} N_j F_{u_z s} P_{u_z} \tag{31}
$$

where $P_{u_\alpha sj} = N_j F_{u_\alpha s} P_{u_\alpha}$, $P_{u_\beta sj} = N_j F_{u_\beta s} P_{u_\beta}$, and $P_{u_z sj} = N_j F_{u_z s} P_{u_z}$.

Thus, equating the virtual works, the following three governing equations are derived:

$$
\begin{aligned}
\delta q_{\alpha_{sj}} &: K_{u_\alpha u_\alpha s\tau ji} q_{\alpha_{\tau i}} + K_{u_\alpha u_\beta s\tau ji} q_{\beta_{\tau i}} + K_{u_\alpha u_z s\tau ji} q_{z_{\tau i}} = P_{u_\alpha sj} \\
\delta q_{\beta_{sj}} &: K_{u_\beta u_\alpha s\tau ji} q_{\alpha_{\tau i}} + K_{u_\beta u_\beta s\tau ji} q_{\beta_{\tau i}} + K_{u_\beta u_z s\tau ji} q_{z_{\tau i}} = P_{u_\beta sj} \\
\delta q_{z_{sj}} &: K_{u_z u_\alpha s\tau ji} q_{\alpha_{\tau i}} + K_{u_z u_\beta s\tau ji} q_{\beta_{\tau i}} + K_{u_z u_z s\tau ji} q_{z_{\tau i}} = P_{u_z sj}
\end{aligned}
\tag{32}
$$

For the sake of completeness, the nine fundamental nuclei of the stiffness matrix are written explicitly in Appendix.

4.3. Stiffness matrix

In this work, the core of the stiffness matrix is the scalar $K_{u_m u_l s\tau ji}$. In the CUF nomenclature, it is named the Fundamental Nucleus (FN). Therefore, the stiffness matrix can be composed of nine independent scalar parameters. This variable-kinematics approach has been proposed in two papers concerning beam and plate formulations (Carrera et al., 2024b, 2025). In contrast, the precedent CUF-based papers (Carrera, 2003) used as the kernel a submatrix $\mathbf{K}_{s\tau ji}$ with dimensions 3×3, where the same expansion theory was used for all the three displacement variables.

In order to explain the differences between the two methods, Fig. 10 is illustrated. In the present method (illustrated in Fig. 10 a), the scalar FN is expanded on s and τ. Subsequently, the resulting submatrix is expanded on u_m and u_l, followed by another expansion on the FE nodes j and i, ultimately yielding the complete structural matrix. On the other hand, Fig. 10 b shows the assembly for the 'classical method'. The loops on the displacement variables are embedded in the 3×3 FN, meaning that $K_{u_m u_l}$ is a component of the matrix $\mathbf{K}_{s\tau ji}$. Then, this nucleus is expanded on s and τ, and subsequently, the resulting submatrix is expanded on j and i, leading to the structural matrix.

Also, for the load vector, the kernel is now a scalar $P_{u_m sj}$. Analogous considerations seen for the stiffness matrix are valid for the load array.

5. Assembly

This section outlines the process of assembling the stiffness matrix and the load vector within the context of the Unified formulation. To

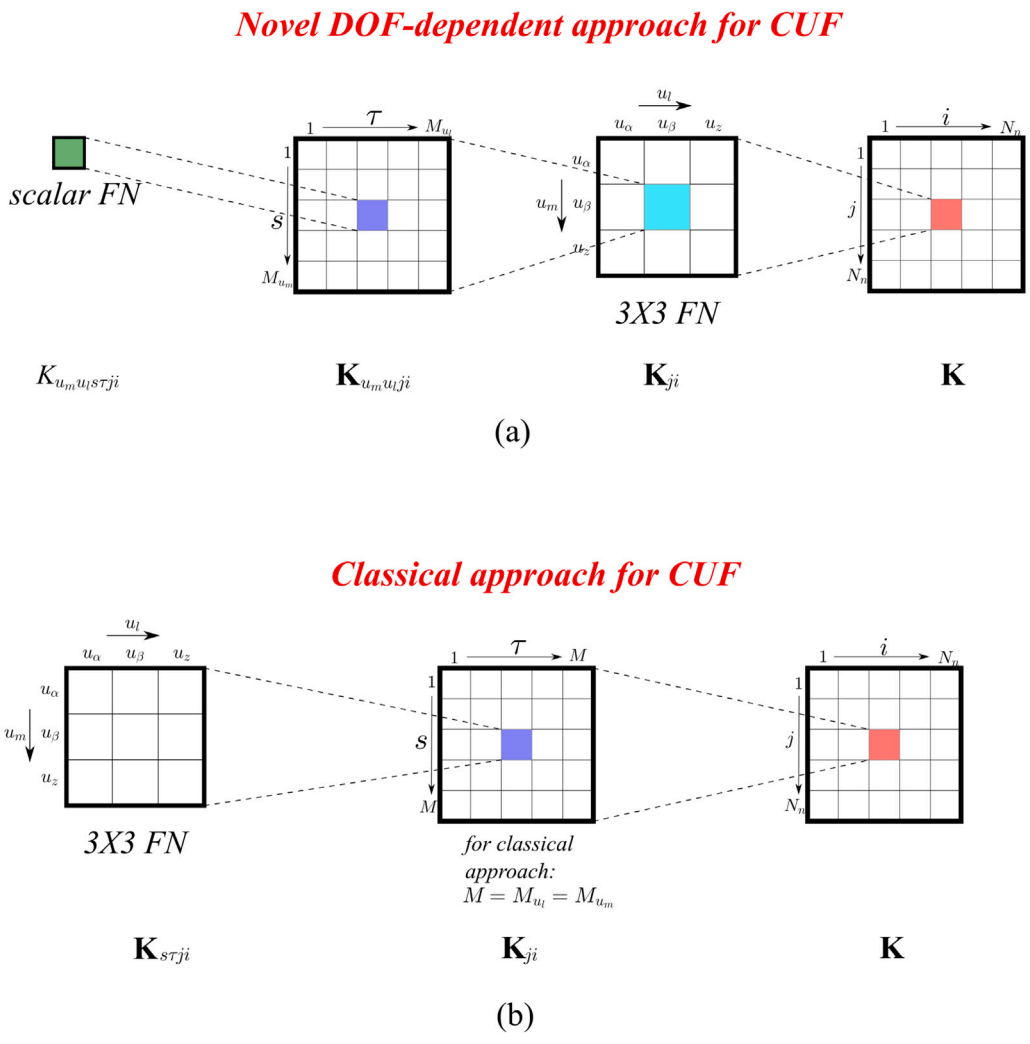

Fig. 10. Assembly of the stiffness matrix for the novel approach (a) and classical CUF (b), starting from the fundamental nuclei.

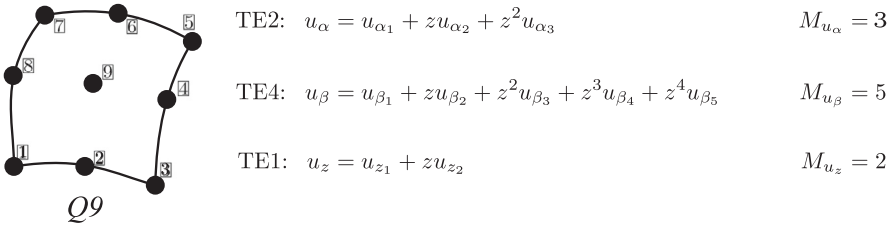

Fig. 11. Example of a shell element. u_α is studied by a second-order models (TE2), u_β is studied by using a fourth-order model (TE4), whereas a linear model (TE1) approximates the displacement field u_z.

illustrate this process, an example is considered. In Fig. 11, a nine-node element (Q9) is depicted. The structural theories employed are also indicated in the figure, where u_α is approximated by a second-order expansion, u_β is modelled using a fourth-order expansion, and u_z is approximated by the TE1 model. Consequently, $M_{u_\alpha} = 3$, $M_{u_\beta} = 5$, and $M_{u_z} = 2$. Thus, 10 degrees of freedom are assigned to each FE node, resulting in a total of ninety degrees of freedom per element. In Fig. 12, the stiffness matrix, with dimensions 90×90, and the load vector, with dimensions 90, for the single element are depicted. Each submatrix $\mathbf{K}_{ji}$ is further divided into nine submatrices, while each subvector $\mathbf{P}_j$ is composed of three smaller subarrays. For instance, Fig. 13 illustrates clearly the nine components of $\mathbf{K}_{11}$ and the three components of $\mathbf{P}_1$. It is important to note that the dimension and shape of the matrices $\mathbf{K}_{u_m u_l 11}$ depend on the number of terms in the models adopted for each displacement variable.

In particular, the three diagonal sub-matrices have a squared shape where:

- $\mathbf{K}_{u_\alpha u_\alpha 11}$ is 3×3;
- $\mathbf{K}_{u_\beta u_\beta 11}$ is 5×5;
- $\mathbf{K}_{u_z u_z 11}$ is 2×2;

The use of different numbers of terms for the variables leads to rectangular sub-matrices $\mathbf{K}_{u_m u_l 11}$ with varying dimensions, as illustrated in the following matrices:

- $\mathbf{K}_{u_\alpha u_\beta 11}$ is 3×5;

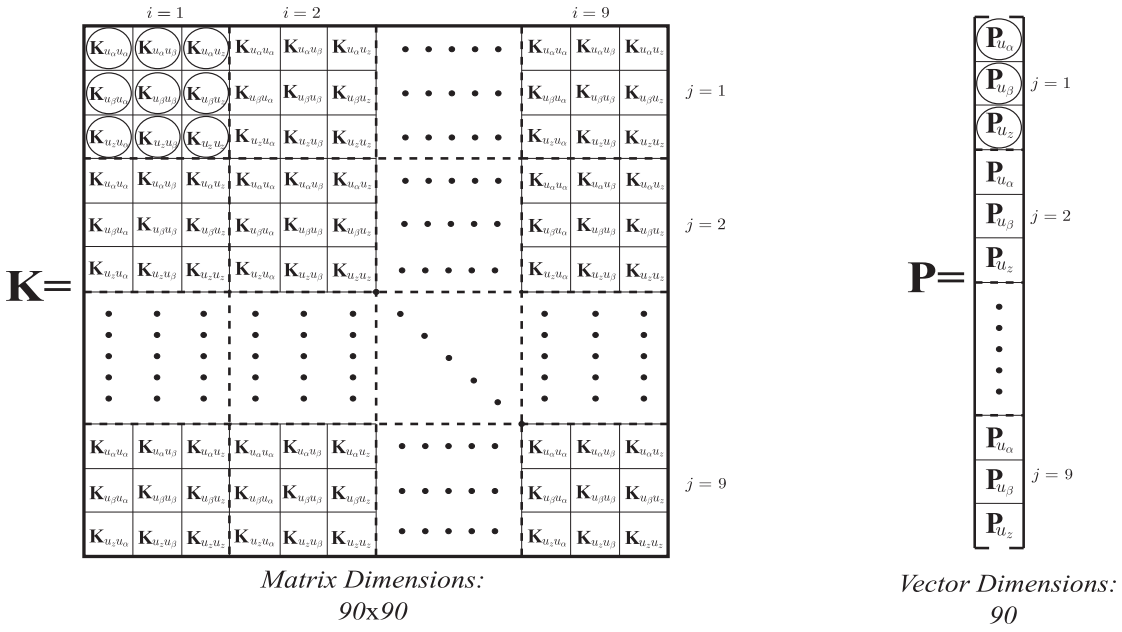

Fig. 12. Assembly of the stiffness matrix and the load vector for a single element.

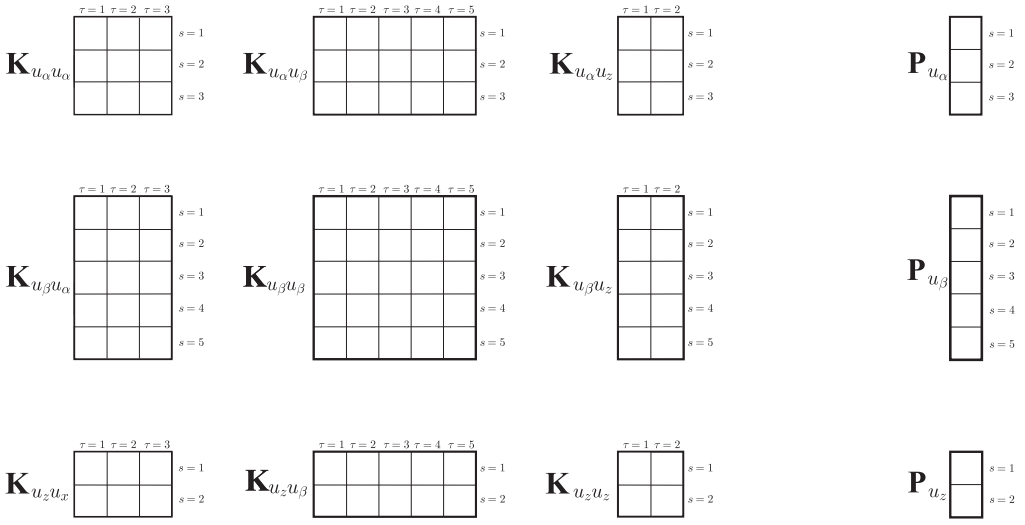

Fig. 13. Assembly of the stiffness matrix (submatrix $\mathbf{K}_{11}$) and the load vector (subvector $\mathbf{P}_1$).

- $\mathbf{K}_{u_\beta u_\alpha}11$ is 5×3;
- $\mathbf{K}_{u_\alpha u_z}11$ is 3×2;
- $\mathbf{K}_{u_z u_\alpha}11$ is 2×3;
- $\mathbf{K}_{u_\beta u_z}11$ is 5×2;
- $\mathbf{K}_{u_z u_\beta}11$ is 2×5;

Each 1×1 scalar FN corresponds to the core of the matrices. A similar procedure can be followed for the load vector.

6. Numerical results

This section investigates three benchmarks with a focus on examining displacements and stresses. The first benchmark involves a cylinder subjected to two pinching forces, followed by a shell with unitary width subjected to sinusoidal bending. A spherical shell loaded by a localized pressure is finally studied. These benchmarks cover various loadings and boundary conditions. Additionally, a range of low-to-high radius-to-thickness ratios are considered. To alleviate the shear and membrane locking issues associated with the finite elements, the MITC integration scheme is employed.

Given that the present method can generate numerous theories, a consistent acronym system is proposed. When referring to both the *uniform* and the *reduced* models, the following notation is adopted: TEn_{u_α}-TEn_{u_β}-TEn_{u_z}, where n_{u_l} denotes the polynomial for each displacement variable. For example, consider Fig. 11. This model might be indicated with TE2-TE4-TE1, where:

- TE2: second-order Taylor expansion for u_α;
- TE4: fourth-order Taylor expansion for u_β;
- TE1: first-order Taylor expansion for u_z.

In some cases, it is useful to use only the constant term. For this expansion, the label TE0 is adopted. When utilizing *reduced* models, the explicit mathematical formulations will be shown for each benchmark.

6.1. Isotropic cylindrical shell under two pinching loads

A cylinder, originally analysed by Lindberg et al. (1969), is taken

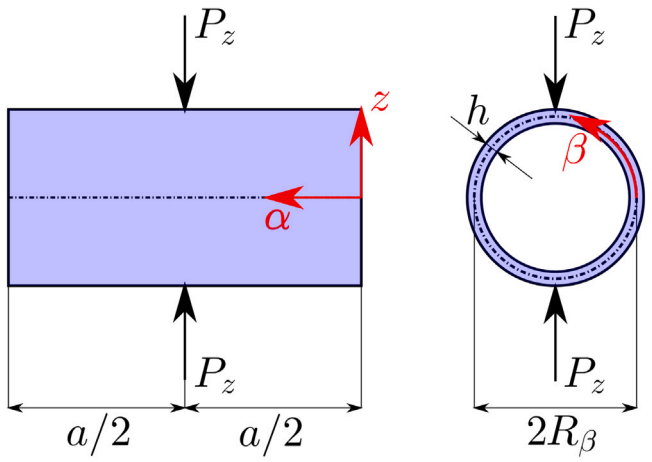

Fig. 14. Geometrical properties and loading conditions of the isotropic cylindrical shell under two pinching loads. The study case is taken from Lindberg et al. (1969).

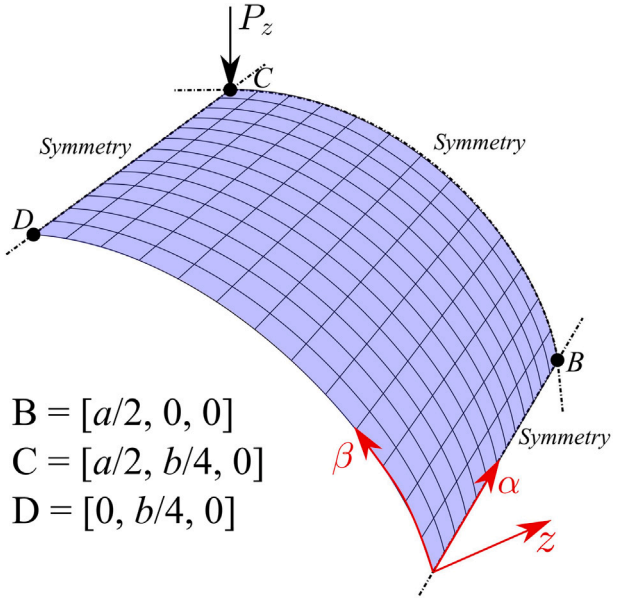

Fig. 15. Isotropic cylindrical shell under two pinching loads. Adoption of a 13 × 13 FEM discretization.

into account as the first benchmark. Fig. 14 depicts the geometrical properties of the structure, with $a/R_\beta = 2$, $R_\beta/h = 100$, and $b = 2\pi R_\beta$. An isotropic material is assumed, with properties: E = 3×10^6 [psi] and $\nu = 0.3$. The cylinder is simply-supported at $\alpha = 0$ and $\alpha = a$. Two pinching loads, P_z, are applied at positions $[a/2, b/4, h/2]$, each with a magnitude of 10^4 [lb]. The results are compared with the analytical solution of Flügge (1934), as calculated by Lindberg et al. (1969). In particular, a double Fourier series solution has been employed, using 80 terms in both mid-surface directions. Additionally, shear forces have been taken into account in the formulation.

Utilizing the symmetry feature of the structure and loading conditions, an octave of the cylinder is studied, as shown in Fig. 15. Thus, the computational time can be reasonably reduced without losing generality. Symmetric boundary conditions are applied. As far as the FE mesh is concerned, a uniform mesh grid of 13 × 13 elements is employed for all the subsequent analyses. The convergence analysis is not shown here for the sake of brevity.

In this case study, transverse displacements, u_z, are investigated, specifically along the lines BC ($[a/2, \beta, 0]$) and DC ($[\alpha, b/4, 0]$), as depicted in Fig. 15. The dimensionless displacements are presented in the following:

$$\bar{u}_z = \frac{Eh}{P_z} u_z \tag{33}$$

Table 3 illustrates the results for the transverse displacements, $\bar{u}_z$, evaluated in point C = $[a/2, b/4, 0]$. The first three columns show the expansions used for the displacement variables. The fourth column displays the number of terms. Then, the results for the displacements are illustrated. Finally, the DOFs are presented for comparison purposes.

These analyses offer an opportunity to underscore the significance of the Poisson locking. This phenomenon arises when TE0 or TE1 expansions are employed for the u_z displacement variable. The Poisson locking is independent from the order used for the variables u_α or u_β. This critical issue can be counteracted using two different strategies:

1. The elastic coefficients are modified. In these analyses, two superscripts are used: 'no Corr' indicates a model where the Poisson Locking is not corrected, while 'Corr' corresponds to models where the correction is applied. See the book Carrera et al. (2014) for more information.
2. Incorporating a parabolic term into the u_z variable is the most appropriate method from a physical point of view, even though with an associated increase in computational costs.

In the first rows, the *uniform* models are compared. It is evident that the model TE3-TE3-TE3 leads to the same results to TE4-TE4-TE4, reaching the convergence for the structural theory. For this reason, the third is the maximum order used of the variables. In the central rows, the *different* models are compared. For the sake of brevity, displacement variables u_α and u_β use the same expansions for each theory. It would be interesting in a following paper to change the expansion individually.

In the last rows, two *reduced* theories are proposed to assess the possibility to ulteriorly reduce the computational costs. The expressions of the model are explicitly given in the following:

$$\text{Model 1:} \quad \begin{aligned} u_\alpha &= u_{\alpha_1} + z u_{\alpha_2} \\ u_\beta &= u_{\beta_1} + z u_{\beta_2} \\ u_z &= u_{z_1} + z^2 u_{z_2} \end{aligned} \tag{34}$$

$$\text{Model 2:} \quad \begin{aligned} u_\alpha &= u_{\alpha_1} + z u_{\alpha_2} + z^3 u_{\alpha_3} \\ u_\beta &= u_{\beta_1} + z u_{\beta_2} + z^3 u_{\beta_3} \\ u_z &= u_{z_1} + z^2 u_{z_2} \end{aligned} \tag{35}$$

Figs. 16 and 17 depict the transverse displacements along the line $[\alpha, b/4, 0]$ and $[a/2, \beta, 0]$, respectively. The leftmost parts of the figures illustrate the reference and uniform solutions. On the other hand, the different and reduced models are shown in the graphs on the rightmost. Also, the figures show that it is possible to use TE3-TE3-TE3 as the reference theory.

Some important remarks based on the results can be outlined:

1. The results are near to the literature solution;
2. The correction of the Poisson locking through the modification of the material coefficients is very effective when TE0 is adopted, while it leads to erroneous results for TE1. On the other hand, the adoption of the parabolic term is interesting, as already stated in the literature;
3. The different and reduced models show their incredible capabilities in reaching excellent results with lower computational costs.

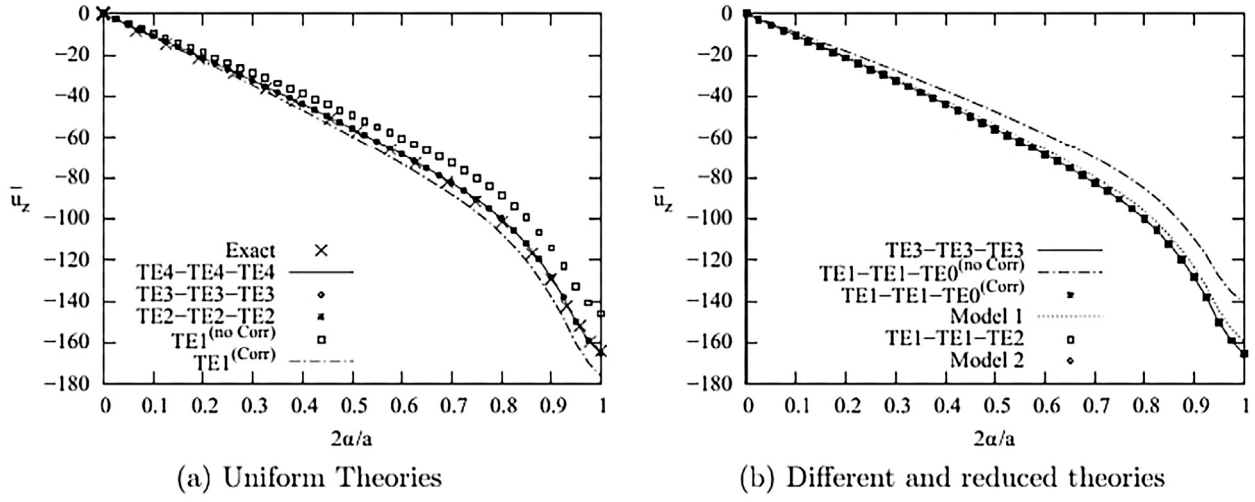

Fig. 16. Isotropic cylindrical shell under two pinching loads. Transverse displacements evaluated along the line DC $[\alpha, b/4, 0]$. Exact result comes from Lindberg et al. (1969).

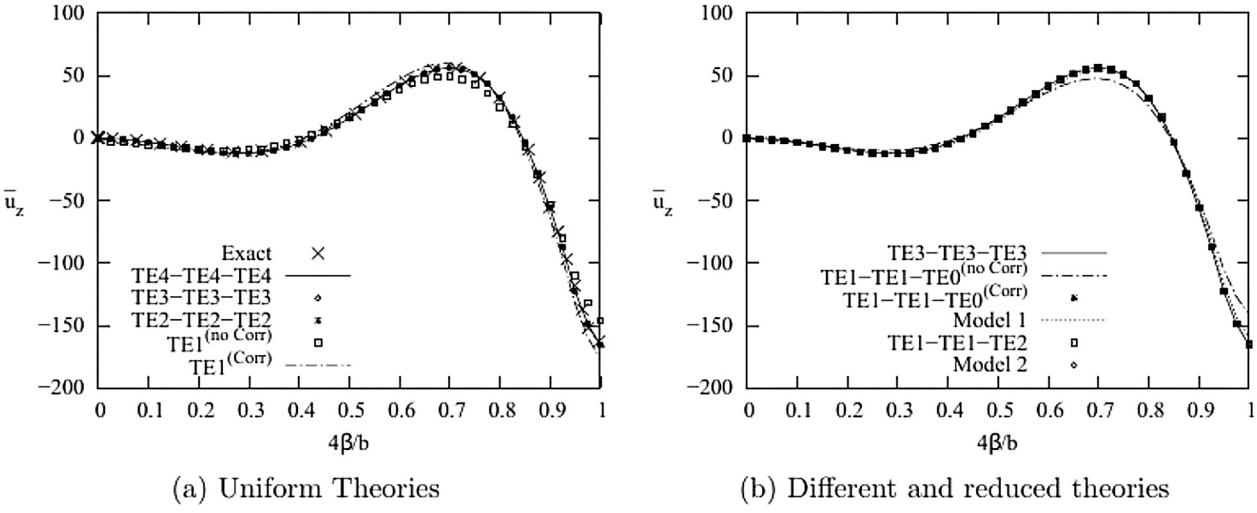

Fig. 17. Isotropic cylindrical shell under two pinching loads. Transverse displacements evaluated along the line BC $[a/2, \beta, 0]$. Exact result comes from Lindberg et al. (1969).

6.2. Cylindrical bending of a shell

A metallic shell is analysed as the second example. This benchmark has already been studied in Carrera et al. (2015). The geometric and loading conditions are described in Fig. 18. Several radius-to-thickness ratios are studied, $R_\beta/h = 4, 10, 50, 100, 1000$. The width a is unitary. The material properties are the: E = 73 [GPa] and $\nu = 0.34$. The shell is simply-supported on the edges along the α-direction, and it is loaded with a sinusoidal pressure$p = p_z \sin\left(\frac{\pi\beta}{b}\right)$, with a mechanical load amplitude of $p_z = 1$ [Pa] at the top position. The study evaluates transverse displacements, u_z, along with in-plane stress, $\sigma_{\beta\beta}$, and shear stress, $\sigma_{\beta z}$. In particular, u_z and $\sigma_{\beta\beta}$ are calculated in $[a/2, b/2, z]$, while $\sigma_{\beta z}$ is evaluated in $[0, b/2, z]$. For comparison purposes, displacements and stresses are given in non-dimensional form as follows:

$$\bar{u}_z = \frac{10\ E\ u_z\ h^3}{p_z\ R_\beta^4} \qquad \bar{\sigma}_{\beta\beta} = \frac{10\ \sigma_{\beta\beta}}{p_z\ \left(\frac{R_\beta}{h}\right)^2} \qquad \bar{\sigma}_{\beta z} = \frac{10\ \sigma_{\beta z}}{p_z\ \left(\frac{R_\beta}{h}\right)} \tag{36}$$

The results are compared with a Navier-type closed-form solution labelled as 'Exact'. Utilizing the strong-form governing equations expressed in the two-dimensional CUF framework, the Navier solution is analytical and employs two sinusoidal functions that exactly satisfy the boundary conditions. This is always achievable in the case of simply-supported structures with no mechanical couplings. A Legendre-based fourth-order uniform model is utilized throughout the thickness. Since this formulation is based on the CUF, the resulting behaviour is 3D-like. The adopted model is highly refined and complete, applying the same kinematic assumptions to all three displacement components. In this way, it accounts for thickness deformation effects. For further details, refer to Carrera (2003).

A convergence mesh analysis is performed for the $R_\beta/h = 100$ case, utilizing TE4-TE4-TE4 as the structural theory. For brevity, the label TE4 is used. Fig. 19 depicts the results in terms of both DOF and number of elements (N° Elements). The 'Exact' model (Carrera et al., 2015) serves as the reference result. Transverse displacements and in-plane stresses are considered as parameters. The results are normalized as follows:

$$u_z^* = \frac{\bar{u}_z}{\bar{u}_z(\text{Exact (Carrera et al., 2015)})}$$
$$\sigma_{\beta\beta}^* = \frac{\bar{\sigma}_{\beta\beta}}{\bar{\sigma}_{\beta\beta}(\text{Exact (Carrera et al., 2015)})} \tag{37}$$

Two integration techniques for the FE functions are compared: the Full scheme (no shear locking correction technique is adopted) and MITC. A mesh discretization of 30 × 1 MITC (equivalent to 2745 DOF for TE4) is selected. This mesh configuration will be utilized for all the radius-to-thickness ratios in the subsequent analyses.

Table 3
Transverse displacements, $\bar{u}_z$, evaluated in $[a/2, b/4, 0]$ for the isotropic cylindrical shell under two pinching loads.

Model u_α	Model u_β	Model u_z	$M_{u_\alpha}/M_{u_\beta}/M_{u_z}$	$\bar{u}_z$	DOF
Exact (Lindberg et al., 1969)					
—	—	—	—[a]	−164.24	—[b]
		Uniform Models			
TE1	TE1	TE1$^{(no\ Corr)}$	2/2/2	−146.07	4374
TE1	TE1	TE1$^{(Corr)}$	2/2/2	−176.45	4374
TE2	TE2	TE2	3/3/3	−165.27	6561
TE3	TE3	TE3	4/4/4	−165.45	8748
TE4	TE4	TE4	5/5/5	−165.45	10 935
		Different Models			
TE0	TE0	TE2	1/1/3	−2.2903	3645
TE0	TE0	TE3	1/1/4	−2.2903	4374
TE1	TE1	TE0$^{(no\ Corr)}$	2/2/1	−140.94	3645
TE1	TE1	TE0$^{(Corr)}$	2/2/1	−165.47	3645
TE1	TE1	TE2	2/2/3	−165.26	5103
TE1	TE1	TE3	2/2/4	−165.27	5832
TE2	TE2	TE0$^{(no\ Corr)}$	3/3/1	−140.94	5103
TE2	TE2	TE0$^{(Corr)}$	3/3/1	−165.47	5103
TE2	TE2	TE1$^{(no\ Corr)}$	3/3/2	−146.07	5832
TE2	TE2	TE1$^{(Corr)}$	3/3/2	−176.45	5832
TE2	TE2	TE3	3/3/4	−165.27	7290
TE3	TE3	TE0$^{(noCorr)}$	4/4/1	−141.17	6561
TE3	TE3	TE0$^{(Corr)}$	4/4/1	−165.70	6561
TE3	TE3	TE1$^{(noCorr)}$	4/4/2	−146.31	7290
TE3	TE3	TE1$^{(Corr)}$	4/4/2	−176.69	7290
TE3	TE3	TE2	4/4/3	−165.45	8019
		Reduced Models			
	Model 1		2/2/2	−159.61	4374
	Model 2		3/3/2	−165.45	6561

[a] M's are not reported for the exact theory.
[b] Analytical solution.

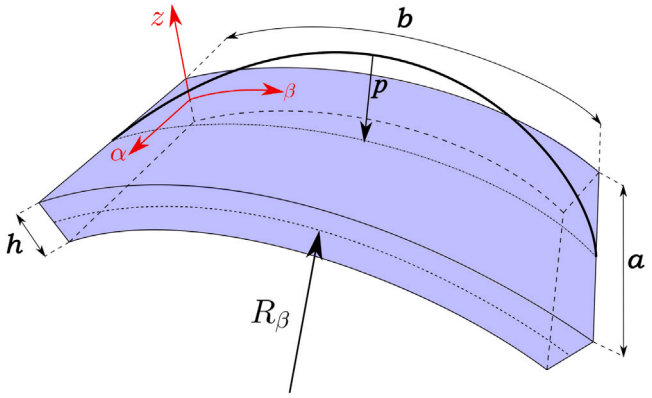

Fig. 18. Geometrical properties of a simply-supported metallic shell under sinusoidal pressure. The benchmark is taken from Carrera et al. (2015).

After selecting the FE discretization, two radius-to-thickness ratios, $R_\beta/h = 4$ and $R_\beta/h = 100$, are considered. Tables 4 and 5 present the results for the thick and thin shell, respectively. The structure of the tables mirrors what was used in the previous example. Specifically, the results for displacements and stresses are provided. Transverse displacements, $\bar{u}_z$, are evaluated at $[a/2, b/2, 0]$. In-plane stresses, $\bar{\sigma}_{\beta\beta}$, and shear stresses, $\bar{\sigma}_{\beta z}$, are calculated at $[a/2, b/2, h/2]$ and $[a, b/2, 0]$, respectively. It should be noted that shear stresses are not present in the literature solution (Carrera et al., 2015). Additionally, in this example, the effect of Poisson Locking is analysed.

In the first rows of the tables, *uniform* models are presented. The *uniform* model TE4-TE4-TE4 can be considered as the present reference solution. In the central rows, *different* models are investigated. Firstly, the influence on u_α is examined, revealing that the constant term is adequate for both R_β/h. Henceforth, TE0 is utilized. Secondly, the influence on u_z is taken into account. Lastly, the study on the impact on u_β demonstrates that higher-order terms are necessary for this displacement variable. Finally, three *reduced theories* are shown in the last part of the table. Their explicit forms are given in the followings:

$$\text{Model 1:} \quad \begin{aligned} u_\alpha &= u_{\alpha_1} \\ u_\beta &= u_{\beta_1} + z u_{\beta_2} \\ u_z &= u_{z_1} + z^2 u_{z_2} + z^3 u_{z_3} \end{aligned} \tag{38}$$

$$\text{Model 2:} \quad \begin{aligned} u_\alpha &= u_{\alpha_1} \\ u_\beta &= u_{\beta_1} + z u_{\beta_2} + z^3 u_{\beta_3} \\ u_z &= u_{z_1} + z^2 u_{z_2} \end{aligned} \tag{39}$$

$$\text{Model 3:} \quad \begin{aligned} u_\alpha &= u_{\alpha_1} \\ u_\beta &= u_{\beta_1} + z u_{\beta_2} + z^3 u_{\beta_3} + z^4 u_{\beta_4} \\ u_z &= u_{z_1} + z u_{z_2} + z^2 u_{z_3} + z^3 u_{z_4} + z^4 u_{z_5} \end{aligned} \tag{40}$$

Even though Model 1 and Model 2 have the same number of terms, the results differ, highlighting the significance of the choice of each term.

Figs. 20 and 21 illustrate the trends of the shear stresses, $\bar{\sigma}_{\beta z}$, in the thick and thin cases, respectively. Some of the most interesting models described previously are reported here.

Finally, Fig. 22 illustrates the relationship between the radius-to-thickness ratio, R_β/h, and the transverse displacement, $\bar{u}_z$, evaluated at $[a/2, b/2, 0]$. It is worth noting that the reduced Model 2 is more accurate than the TE2 model despite having fewer DOF.

The results lead to the following observations:

1. The analysis highlights the necessity to use higher-order terms to determine the outcomes accurately;
2. Using different and reduced models is proved to be an incredible method for choosing the best compromise between accuracy and computational costs;
3. It is notable that the constant term for the displacement variable u_α is sufficient. The terms of the in-plane displacement field u_β are the most influential in the solution. Conversely, the problem demonstrates less sensitivity to the model for u_z.
4. The behaviour of the outputs $\bar{u}_z$ and $\bar{\sigma}_{\beta\beta}$ is significantly influenced by the ratio R_β/h. Indeed, several terms are required to achieve excellent results for thick shells, whereas few DOF are adequate for thin structures. However, the shear stresses, $\bar{\sigma}_{\beta z}$, exhibit almost identical trends for the two considered radius-to-thickness ratios.

6.3. Isotropic spherical shell loaded by a localized pressure

A simply-supported spherical shell is analysed as the final example. This case could be used in the future as a benchmark. The geometrical and loading conditions are outlined in Fig. 23. The shell is subjected to a constant pressure applied in a relatively small zone located at the top centre The area has dimensions of 5×5 [mm^2], while the module of the pressure is equal to 1 [MPa]. The shell's geometric parameters are $a = 100$ [mm], $b = 100$ [mm], $h = 6$ [mm], and the radii of curvature are $R = R_\alpha = R_\beta = 100$ [mm]. The material properties are chosen as follows: $E = 70$ [GPa], $G = 26$ [GPa], $\nu = 0.3$. A quarter of the shell may be considered due to the symmetries of the problems. Transverse displacements, u_z, and in-plane stresses, $\sigma_{\alpha\alpha}$, are evaluated. It is useful to use a non-dimensionalized form, given in the following:

$$\bar{u}_z = \frac{100\ E\ u_z}{p\left(\frac{R}{h}\right)^2 h} \qquad \bar{\sigma}_{\alpha\alpha} = \frac{100\ \sigma_{\alpha\alpha}}{p\left(\frac{R}{h}\right)^2} \tag{41}$$

A non-uniform mesh grid of 38×38 elements is employed in the following analyses. Due to space constraints, the convergence analysis is not explicitly presented.

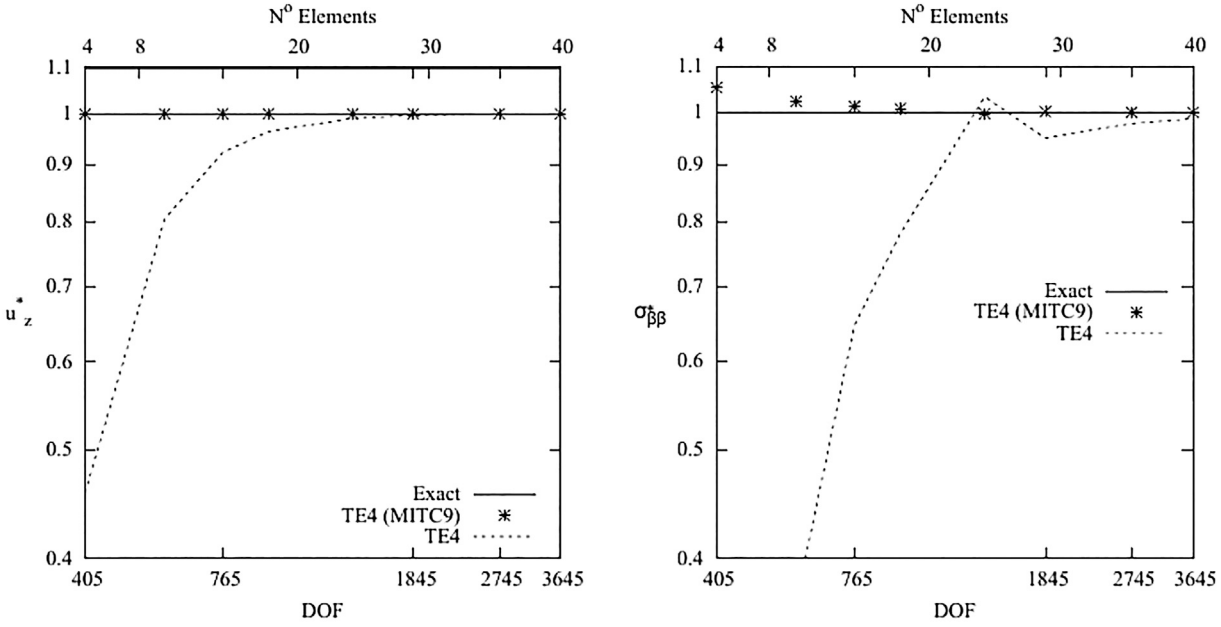

(a) Transverse displacement in $[a/2, b/2, 0]$. (b) In-plane stress in $[a/2, b/2, h/2]$.

Fig. 19. Simply-supported metallic shell under sinusoidal pressure. Case $a/h = 100$. Convergence analysis. Exact result comes from Carrera et al. (2015).

Table 4
Simply-supported metallic shell under sinusoidal pressure. Case $a/h = 4$.

Model u_α	Model u_β	Model u_z	$M_{u_\alpha}/M_{u_\beta}/M_{u_z}$	$\bar{u}_z$ [a]	$\bar{\sigma}_{\beta\beta}$ [b]	$\bar{\sigma}_{\beta z}$ [c]	DOF
			Exact (Carrera et al., 2015)				
LD4	LD4	LD4	—[d]	2.1213	2.7722	—	—[e]
			Uniform Models				
TE1	TE1	TE1$^{(noCorr)}$	2/2/2	1.6208	3.8366	4.2009	1098
TE1	TE1	TE1$^{(Corr)}$	2/2/2	2.1112	2.5372	4.2009	1098
TE2	TE2	TE2	3/3/3	2.0763	2.3702	4.5210	1647
TE3	TE3	TE3	4/4/4	2.1210	2.9343	6.2516	2196
TE4	TE4	TE4	5/5/5	2.1214	2.7758	6.2673	2745
			Different models (Influence on u_α)				
TE0	TE4	TE4	1/5/5	2.1214	2.7758	6.2673	2013
			Different models (Influence on u_z)				
TE0	TE4	TE0$^{(noCorr)}$	1/5/1	1.6730	3.9778	6.2588	1281
TE0	TE4	TE0$^{(Corr)}$	1/5/1	2.1637	2.5999	6.2679	1281
TE0	TE4	TE1$^{(noCorr)}$	1/5/2	1.6725	3.9851	6.2589	1464
TE0	TE4	TE1$^{(Corr)}$	1/5/2	2.1631	2.6108	6.2679	1464
TE0	TE4	TE2	1/5/3	2.1124	2.5074	6.2539	1647
TE0	TE4	TE3	1/5/4	2.1214	2.9264	6.2564	1830
			Different models (Influence on u_β)				
TE0	TE0	TE4	1/1/5	0.2779	0.1866	4.1981	1281
TE0	TE1	TE4	1/2/5	2.0857	2.7403	4.5268	1464
TE0	TE2	TE4	1/3/5	2.0856	2.7463	4.5220	1647
TE0	TE3	TE4	1/4/5	2.1210	2.7831	6.2626	1830
			Reduced Models				
	Model 1		1/2/3	2.0825	2.7173	4.5336	1098
	Model 2		1/3/2	2.1135	2.4378	6.2577	1098
	Model 3		1/4/5	2.1211	2.7799	6.2696	1830

[a] Computed at $[a/2, b/2, 0]$.
[b] Computed at $[a/2, b/2, h/2]$.
[c] Computed at $[a/2, 0, 0]$.
[d] M's are not reported for the exact theory
[e] Closed-form solution.

First, Table 6 illustrates the transverse displacements, u_z, and the in-plane stresses, $\sigma_{\alpha\alpha}$, both calculated in $[a/2, b/2, h/2]$. The reference solution is the complete theory TE4-TE4-TE4. In this example, only the 'corrected' strategy for TE1-TE1-TE1 is used. In this way, the upperscript 'Corr' may be omitted for conciseness. Due to space constraints, uniform, and reduced models are taken into account. Three reduced theories are chosen. Their mathematical expressions are given as follows:

$$\text{Model 1:} \quad \begin{aligned} u_\alpha &= u_{\alpha_1} + z u_{\alpha_2} \\ u_y &= u_{\beta_1} + z u_{\beta_2} \\ u_z &= u_{z_1} + z u_{z_2} + z^2 u_{z_3} \\ u_x &= u_{\alpha_1} + z u_{\alpha_2} + z^2 u_{\alpha_3} + z^4 u_{\alpha_4} \end{aligned} \tag{42}$$

Table 5
Simply-supported metallic shell under sinusoidal pressure. Case $a/h = 100$.

Model u_α	Model u_β	Model u_z	$M_{u_\alpha}/M_{u_\beta}/M_{u_z}$	$\overline{u}_z$ [a]	$\overline{\sigma}_{\beta\beta}$ [b]	$\overline{\sigma}_{\beta z}$ [c]	DOF
			Exact (Carrera et al., 2015)				
LD4	LD4	LD4	—[d]	1.6669	2.5504	—	—[e]
			Uniform Models				
TE1	TE1	TE1$^{(noCorr)}$	2/2/2	1.2247	3.8626	3.7722	1098
TE1	TE1	TE1$^{(Corr)}$	2/2/2	1.6669	2.5456	3.7722	1098
TE2	TE2	TE2	3/3/3	1.6669	2.5346	4.0922	1647
TE3	TE3	TE3	4/4/4	1.6669	2.5528	5.6576	2196
TE4	TE4	TE4	5/5/5	1.6669	2.5525	5.6577	2745
			Different models (Influence on u_α)				
TE0	TE4	TE4	1/5/5	1.6669	2.5525	5.6577	2013
			Different models (Influence on u_z)				
TE0	TE4	TE0$^{(noCorr)}$	1/5/1	1.2247	3.8670	5.6582	1281
TE0	TE4	TE0$^{(Corr)}$	1/5/1	1.6670	2.5522	5.6582	1281
TE0	TE4	TE1$^{(noCorr)}$	1/5/2	1.2247	3.8629	5.6582	1464
TE0	TE4	TE1$^{(Corr)}$	1/5/2	1.6670	2.5457	5.6582	1464
TE0	TE4	TE2	1/5/3	1.6669	2.5349	5.6576	1647
TE0	TE4	TE3	1/5/4	1.6669	2.5528	5.6576	1830
			Different models (Influence on u_β)				
TE0	TE0	TE4	1/1/5	0.0004	0.0038	3.7721	1281
TE0	TE1	TE4	1/2/5	1.6669	2.5524	4.0922	1464
TE0	TE2	TE4	1/3/5	1.6669	2.5524	4.0922	1647
TE0	TE3	TE4	1/4/5	1.6669	2.5525	5.6577	1830
			Reduced Models				
	Model 1		1/2/3	1.6669	2.5525	4.0922	1098
	Model 2		1/3/2	1.6669	2.5525	5.6576	1098
	Model 3		1/4/5	1.6669	2.5525	5.6577	1830

[a] Computed at $[a/2, b/2, 0]$.
[b] Computed at $[a/2, b/2, h/2]$.
[c] Computed at $[a/2, 0, 0]$.
[d] M's are not reported for the exact theory.
[e] Closed-form solution.

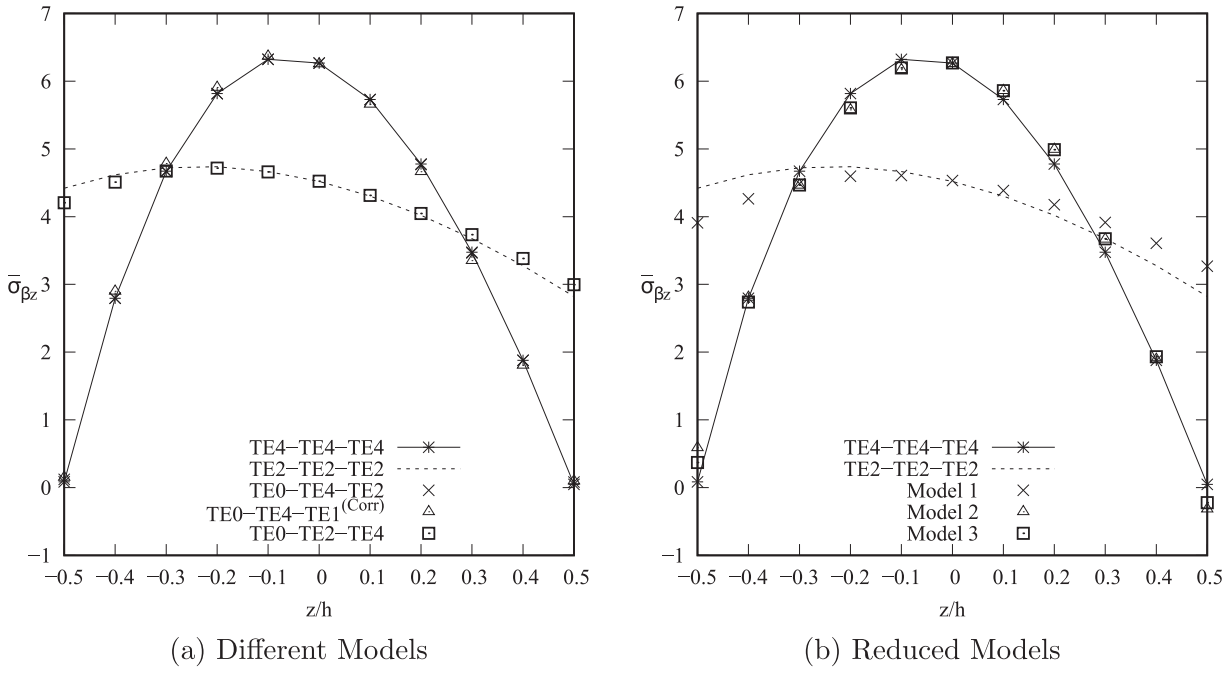

Fig. 20. Simply-supported metallic shell under sinusoidal pressure. Case $a/h = 4$. Shear stresses, $\overline{\sigma}_{\beta z}$, evaluated in $[a/2, 0, z]$.

Model 2:
$$u_y = u_{\beta_1} + zu_{\beta_2} \qquad (43)$$
$$u_z = u_{z_1} + zu_{z_2} + z^2 u_{z_3}$$

Model 3:
$$u_x = u_{\alpha_1} + zu_{\alpha_2} + z^2 u_{\alpha_3} + z^4 u_{\alpha_4}$$
$$u_\beta = u_{\beta_1} + zu_{\beta_2} + z^2 u_{\beta_3} + z^3 u_{\beta_4} \qquad (44)$$
$$u_z = u_{z_1} + zu_{z_2} + z^2 u_{z_3}$$

Second, Fig. 24 shows the trends of the transverse displacements for the uniform and the reduced models along the line $[\alpha, b/2, h/2]$. A magnifier may be used to clarify the situation near the loading part. Instead, Fig. 25 depicts the in-plane stresses.

Some final conclusions may be drawn as follows:

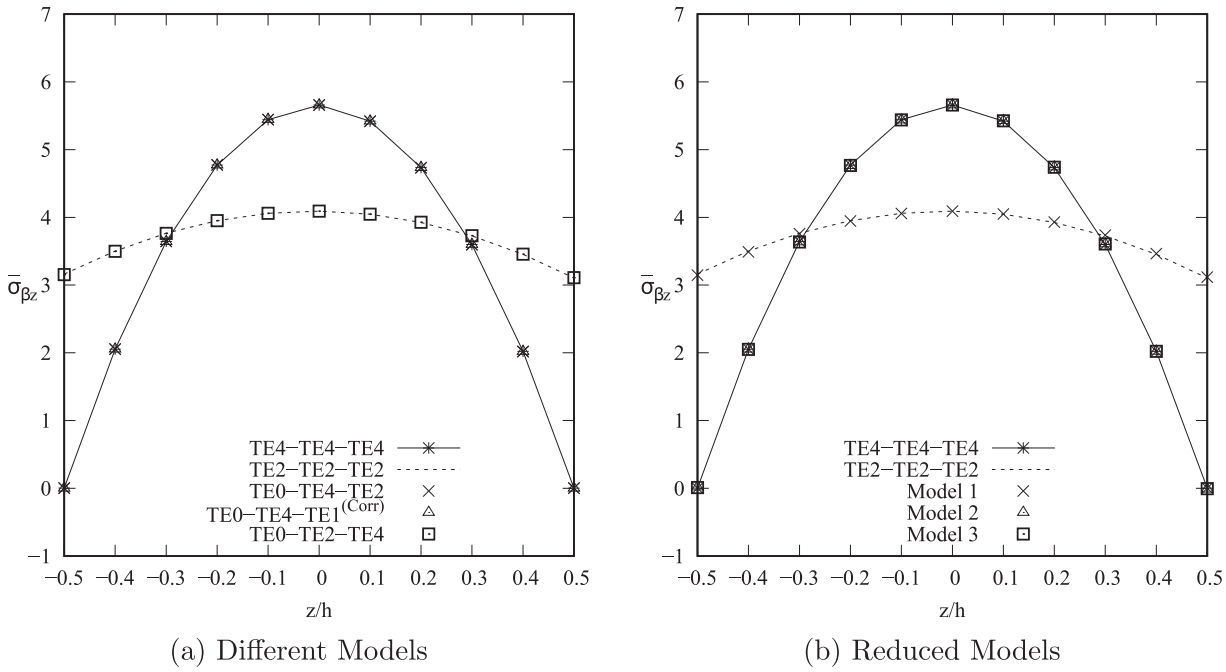

Fig. 21. Simply-supported metallic shell under sinusoidal pressure. Case $a/h = 100$. Shear stresses, $\overline{\sigma}_{\beta z}$, evaluated in $[a/2, 0, z]$.

Table 6
Spherical shell loaded by localized distribution of pressure. Transverse displacements are evaluated in $[a/2, b/2, h/2]$.

Model u_α	Model u_β	Model u_z	$M_{u_\alpha}/M_{u_\beta}/M_{u_z}$	$-\overline{u}_z$	$-\overline{\sigma}_{\alpha\alpha}$	DOF
			Uniform Models			
TE1	TE1	TE1	2/2/2	2.290	0.403	35 574
TE2	TE2	TE2	3/3/3	2.085	0.530	53 361
TE3	TE3	TE3	4/4/4	2.123	0.617	71 148
TE4	TE4	TE4	5/5/5	2.126	0.585	88935[a]
			Reduced Models			
Model 1			2/2/3	2.075	0.449	41 503
Model 2			4/2/3	2.099	0.568	53 361
Model 3			4/4/3	2.123	0.625	65 219

[a] Taken as the reference solution.

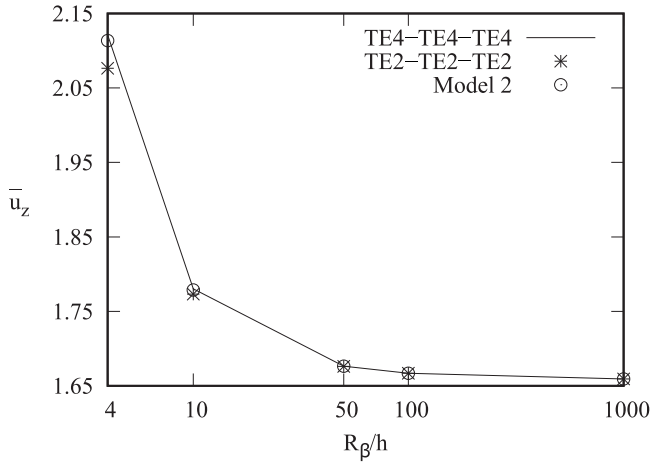

Fig. 22. Simply-supported metallic shell under sinusoidal pressure. Relationship between radius-to-thickness ratio, R_β/h, and the transverse displacement, $\overline{u}_z$ (evaluated in $[a/2, b/2, 0]$).

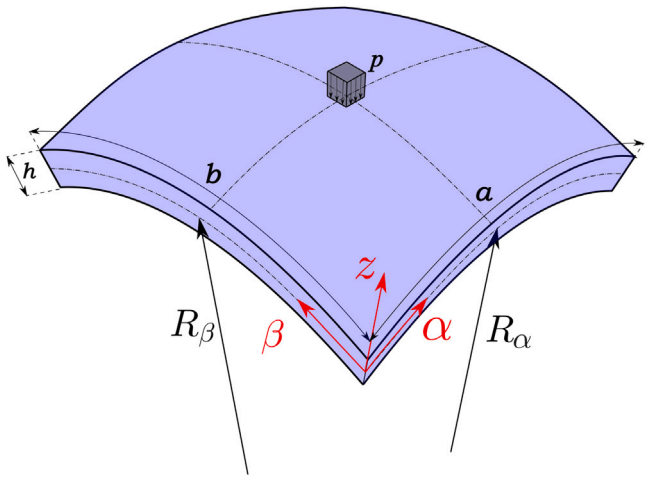

Fig. 23. Geometrical properties of a simply-supported spherical shell loaded by a localized constant pressure.

1. Higher-order terms become necessary to accurately capture the behaviour in the vicinity of the loaded area. This holds especially true when analysing in-plane stresses;
2. When investigating stresses, the in-plane displacement variable, u_α, significantly influences the results;

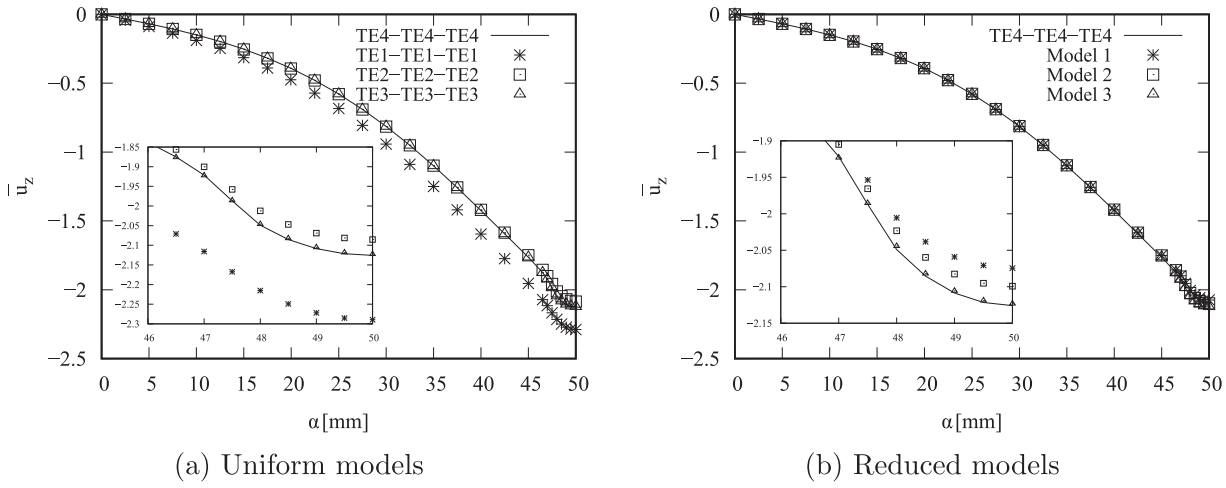

Fig. 24. Spherical shell loaded by localized distribution of pressure. Transverse displacements, u_z, are evaluated along $[\alpha, b/2, h/2]$.

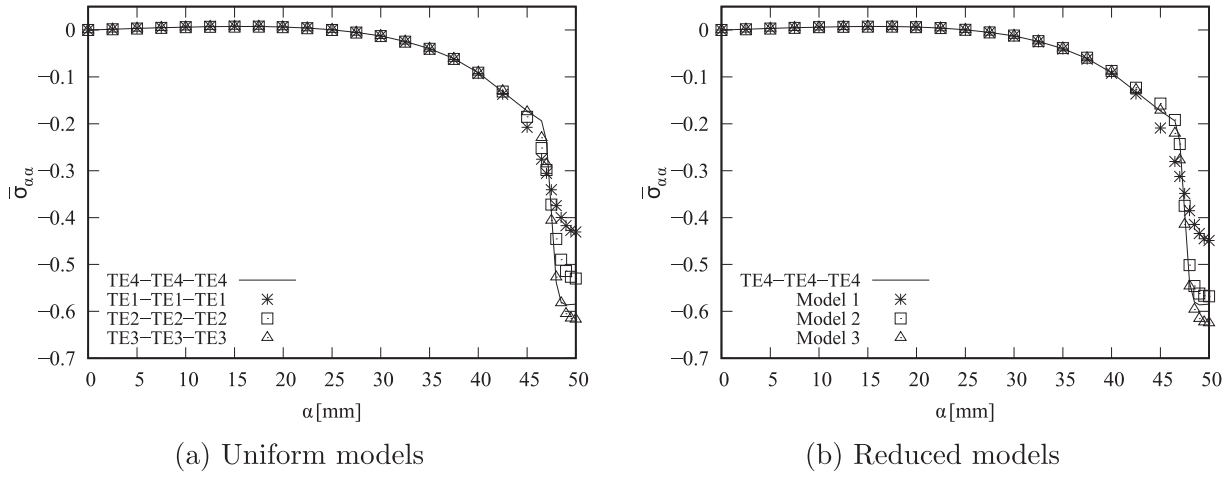

Fig. 25. Spherical shell loaded by localized distribution of pressure. In-plane stresses, $\sigma_{\alpha\alpha}$, are evaluated along $[\alpha, b/2, h/2]$.

3. The example highlights the potential to utilize only relevant terms to attain significant results. In particular, reduced models 2 and 3 prove useful for determining stresses.

7. Conclusions

In this paper, a novel approach to constructing shell theories have been introduced within the framework of the Carrera Unified Formulation (CUF). This approach allows for the development of dedicated structural theories for each displacement variable, enabling the creation of two-dimensional finite element models tailored to study various structures. Additionally, the MITC method is incorporated into the framework. The current study marks the initial step of a series of papers aimed at developing a method for determining the best theories, as discussed in Section 1. Three case studies have been conducted, two drawn from open literature, all within the context of isotropic materials and simply-supported boundary conditions. Several thicknesses have been considered. The results have been compared with existing literature solutions and the CUF-based uniform solutions, leading to the following conclusions:

1. It is feasible to significantly reduce computational costs by selectively utilizing only the most relevant terms within the structural theories;
2. The choice of the appropriate kinematics model is contingent upon the structure geometry and the specific loading conditions. Relevant is the difference between thin and thick structures;
3. The use of the MITC method is indeed of paramount importance if thin structures are considered;
4. The choice of the relevant terms depends on which parameter is studied. It is shown, for instance, that more terms are needed for determining the shear stresses.
5. The number of effective variables is highly dependent on the nature of the problem under consideration.

Several possibilities are under development in future works. Currently, a preliminary paper on shell multi-layered structures (Carrera and Scano, 2024) has been recently proposed. It would also be possible to perform multi-field analyses, e.g., thermoelastic or piezoelectric ones.

CRediT authorship contribution statement

D. Scano: Visualization, Investigation, Writing – review & editing, Data curation, Writing – original draft, Software, Formal analysis. **E. Carrera:** Writing – review & editing, Funding acquisition, Conceptualization, Resources, Formal analysis, Supervision, Project administration. **E. Zappino:** Software, Visualization, Conceptualization, Supervision, Writing – review & editing.

Declaration of competing interest

The authors declare that they have no known competing financial interests or personal relationships that could have appeared to influence the work reported in this paper.

Appendix. Explicit expression of the nine fundamental nuclei

$$
\begin{aligned}
K_{u_\alpha u_\alpha s\tau ji} = {} & C_{11} N_{j,\alpha}^{n1} N_{i,\alpha}^{m1} \int_\Omega N_{n1} N_{m1} \mathrm{d}\alpha\mathrm{d}\beta \int_A F_{u_\alpha s} F_{u_\alpha \tau} \frac{H_\beta}{H_\alpha} \mathrm{d}z \\
& + C_{55} N_j^{n1} N_i^{m1} \int_\Omega N_{n1} N_{m1} \mathrm{d}\alpha\mathrm{d}\beta \int_A F_{u_\alpha s,z} F_{u_\alpha \tau,z} H_\alpha H_\beta \mathrm{d}z \\
& - C_{55} \frac{1}{R_\alpha} N_j^{n1} N_i^{m1} \int_\Omega N_{n1} N_{m1} \mathrm{d}\alpha\mathrm{d}\beta \int_A F_{u_\alpha s,z} F_{u_\alpha \tau} H_\beta \mathrm{d}z \\
& - C_{55} \frac{1}{R_\alpha} N_j^{n1} N_i^{m1} \int_\Omega N_{n1} N_{m1} \mathrm{d}\alpha\mathrm{d}\beta \int_A F_{u_\alpha s} F_{u_\alpha \tau,z} H_\beta \mathrm{d}z \\
& + C_{55} \frac{1}{R_\alpha^2} N_j^{n1} N_i^{m1} \int_\Omega N_{n1} N_{m1} \mathrm{d}\alpha\mathrm{d}\beta \int_A F_{u_\alpha s} F_{u_\alpha \tau} \frac{H_\beta}{H_\alpha} \mathrm{d}z \\
& + C_{66} N_{j,\beta}^{n3} N_{i,\beta}^{m3} \int_\Omega N_{n3} N_{m3} \mathrm{d}\alpha\mathrm{d}\beta \int_A F_{u_\alpha s} F_{u_\alpha \tau} \frac{H_\alpha}{H_\beta} \mathrm{d}z
\end{aligned} \tag{45}
$$

$$
\begin{aligned}
K_{u_\alpha u_\beta s\tau ji} = {} & C_{12} N_{j,\beta}^{n2} N_{i,\alpha}^{m1} \int_\Omega N_{n2} N_{m1} \mathrm{d}\alpha\mathrm{d}\beta \int_A F_{u_\alpha s} F_{u_\beta \tau} \mathrm{d}z \\
& + C_{66} N_{j,\alpha}^{n3} N_{i,\beta}^{m3} \int_\Omega N_{n3} N_{m3} \mathrm{d}\alpha\mathrm{d}\beta \int_A F_{u_\alpha s} F_{u_\beta \tau} \mathrm{d}z
\end{aligned} \tag{46}
$$

$$
\begin{aligned}
K_{u_\alpha u_z s\tau ji} = {} & C_{11} \frac{1}{R_\alpha} N_j^{n1} N_{i,\alpha}^{m1} \int_\Omega N_{n1} N_{m1} \mathrm{d}\alpha\mathrm{d}\beta \int_A F_{u_\alpha s} F_{u_z \tau} \frac{H_\beta}{H_\alpha} \mathrm{d}z \\
& + C_{12} \frac{1}{R_\beta} N_j^{n2} N_{i,\alpha}^{m1} \int_\Omega N_{n2} N_{m1} \mathrm{d}\alpha\mathrm{d}\beta \int_A F_{u_\alpha s} F_{u_z \tau} \mathrm{d}z \\
& + C_{13} N_{i,\alpha}^{m1} \int_\Omega N_j N_{m1} \mathrm{d}\alpha\mathrm{d}\beta \int_A F_{u_\alpha s,z} F_{u_z \tau} H_\beta \mathrm{d}z \\
& + C_{55} N_{j,\alpha}^{n1} N_i^{m1} \int_\Omega N_{n1} N_{m1} \mathrm{d}\alpha\mathrm{d}\beta \int_A F_{u_\alpha s} F_{u_z \tau,z} H_\beta \mathrm{d}z \\
& - C_{55} \frac{1}{R_\alpha} N_{j,\alpha}^{n1} N_i^{m1} \int_\Omega N_{n1} N_{m1} \mathrm{d}\alpha\mathrm{d}\beta \int_A F_{u_\alpha s} F_{u_z \tau} \frac{H_\beta}{H_\alpha} \mathrm{d}z
\end{aligned} \tag{47}
$$

$$
\begin{aligned}
K_{u_\beta u_\alpha s\tau ji} = {} & C_{12} N_{j,\alpha}^{n1} N_{i,\beta}^{m2} \int_\Omega N_{n1} N_{m2} \mathrm{d}\alpha\mathrm{d}\beta \int_A F_{u_\beta s} F_{u_\alpha \tau} \mathrm{d}z \\
& + C_{66} N_{j,\beta}^{n3} N_{i,\alpha}^{m3} \int_\Omega N_{n3} N_{m3} \mathrm{d}\alpha\mathrm{d}\beta \int_A F_{u_\beta s} F_{u_\alpha \tau} \mathrm{d}z
\end{aligned} \tag{48}
$$

$$
\begin{aligned}
K_{u_\beta u_\beta s\tau ji} = {} & C_{22} N_{j,\beta}^{n2} N_{i,\beta}^{m2} \int_\Omega N_{n2} N_{m2} \mathrm{d}\alpha\mathrm{d}\beta \int_A F_{u_\beta s} F_{u_\beta \tau} \frac{H_\alpha}{H_\beta} \mathrm{d}z \\
& + C_{44} N_j^{n2} N_i^{m2} \int_\Omega N_{n2} N_{m2} \mathrm{d}\alpha\mathrm{d}\beta \int_A F_{u_\beta s,z} F_{u_\beta \tau,z} H_\alpha H_\beta \mathrm{d}z \\
& - C_{44} \frac{1}{R_\beta} N_j^{n2} N_i^{m2} \int_\Omega N_{n2} N_{m2} \mathrm{d}\alpha\mathrm{d}\beta \int_A F_{u_\beta s} F_{u_\beta \tau,z} H_\alpha \mathrm{d}z \\
& - C_{44} \frac{1}{R_\beta} N_j^{n2} N_i^{m2} \int_\Omega N_{n2} N_{m2} \mathrm{d}\alpha\mathrm{d}\beta \int_A F_{u_\beta s,z} F_{u_\beta \tau} H_\alpha \mathrm{d}z \\
& + C_{44} \frac{1}{R_\beta^2} N_j^{n2} N_i^{m2} \int_\Omega N_{n2} N_{m2} \mathrm{d}\alpha\mathrm{d}\beta \int_A F_{u_\beta s} F_{u_\beta \tau} \frac{H_\alpha}{H_\beta} \mathrm{d}z \\
& + C_{66} N_{j,\alpha}^{n3} N_{i,\alpha}^{m3} \int_\Omega N_{n3} N_{m3} \mathrm{d}\alpha\mathrm{d}\beta \int_A F_{u_\beta s} F_{u_\beta \tau} \frac{H_\beta}{H_\alpha} \mathrm{d}z
\end{aligned} \tag{49}
$$

$$
\begin{aligned}
K_{u_\beta u_z s\tau ji} = {} & C_{12} \frac{1}{R_\alpha} N_j^{n1} N_{i,\beta}^{m2} \int_\Omega N_{n1} N_{m2} \mathrm{d}\alpha\mathrm{d}\beta \int_A F_{u_\beta s} F_{u_z \tau} \mathrm{d}z \\
& + C_{22} \frac{1}{R_\beta} N_j^{n2} N_{i,\beta}^{m2} \int_\Omega N_{n2} N_{m2} \mathrm{d}\alpha\mathrm{d}\beta \int_A F_{u_\beta s} F_{u_z \tau} \frac{H_\alpha}{H_\beta} \mathrm{d}z \\
& + C_{23} N_{i,\beta}^{m2} \int_\Omega N_j N_{m2} \mathrm{d}\alpha\mathrm{d}\beta \int_A F_{u_\beta s,z} F_{u_z \tau} H_\alpha \mathrm{d}z \\
& + C_{44} N_{j,\beta}^{n2} N_i^{m2} \int_\Omega N_{n2} N_{m2} \mathrm{d}\alpha\mathrm{d}\beta \int_A F_{u_\beta s} F_{u_z \tau,z} H_\alpha \mathrm{d}z
\end{aligned} \tag{50}
$$

$$
\begin{aligned}
K_{u_z u_\alpha s\tau ji} = {} & C_{11} \frac{1}{R_\alpha} N_{j,\alpha}^{n1} N_i^{m1} \int_\Omega N_{n1} N_{m1} \mathrm{d}\alpha\mathrm{d}\beta \int_A F_{u_z s} F_{u_\alpha \tau} \frac{H_\beta}{H_\alpha} \mathrm{d}z \\
& + C_{12} \frac{1}{R_\beta} N_{j,\alpha}^{n1} N_i^{m2} \int_\Omega N_{n1} N_{m2} \mathrm{d}\alpha\mathrm{d}\beta \int_A F_{u_z s} F_{u_\alpha \tau} \mathrm{d}z \\
& + C_{13} N_{j,\alpha}^{n1} \int_\Omega N_{n1} N_i \mathrm{d}\alpha\mathrm{d}\beta \int_A F_{u_z s} F_{u_\alpha \tau,z} H_\beta \mathrm{d}z \\
& + C_{55} N_j^{n1} N_{i,\alpha}^{m1} \int_\Omega N_{n1} N_{m1} \mathrm{d}\alpha\mathrm{d}\beta \int_A F_{u_z s,z} F_{u_\alpha \tau} H_\beta \mathrm{d}z \\
& - C_{55} \frac{1}{R_\alpha} N_j^{n1} N_{i,\alpha}^{m1} \int_\Omega N_{n1} N_{m1} \mathrm{d}\alpha\mathrm{d}\beta \int_A F_{u_z s} F_{u_\alpha \tau} \frac{H_\beta}{H_\alpha} \mathrm{d}z
\end{aligned} \tag{51}
$$

$$
\begin{aligned}
K_{u_z u_\beta s\tau ji} = {} & C_{12} \frac{1}{R_\alpha} N_{j,\beta}^{n2} N_i^{m1} \int_\Omega N_{n2} N_{m1} \mathrm{d}\alpha\mathrm{d}\beta \int_A F_{u_z s} F_{u_\beta \tau} \mathrm{d}z \\
& + C_{22} \frac{1}{R_\beta} N_{j,\beta}^{n2} N_i^{m2} \int_\Omega N_{n2} N_{m2} \mathrm{d}\alpha\mathrm{d}\beta \int_A F_{u_z s} F_{u_\beta \tau} \frac{H_\alpha}{H_\beta} \mathrm{d}z \\
& + C_{23} N_{j,\beta}^{n2} \int_\Omega N_{n2} N_i \mathrm{d}\alpha\mathrm{d}\beta \int_A F_{u_z s} F_{u_\beta \tau,z} H_\alpha \mathrm{d}z \\
& + C_{44} N_j^{n2} N_{i,beta}^{m2} \int_\Omega N_{n2} N_{m2} \mathrm{d}\alpha\mathrm{d}\beta \int_A F_{u_z s,z} F_{u_\beta \tau} H_\alpha \mathrm{d}z \\
& - C_{44} \frac{1}{R_\beta} N_j^{n2} N_{i,beta}^{m2} \int_\Omega N_{n2} N_{m2} \mathrm{d}\alpha\mathrm{d}\beta \int_A F_{u_z s} F_{u_\beta \tau} \frac{H_\alpha}{H_\beta} \mathrm{d}z
\end{aligned} \tag{52}
$$

$$
\begin{aligned}
K_{u_z u_z s\tau ji} = {} & C_{11} \frac{1}{R_\alpha^2} N_j^{n1} N_i^{m1} \int_\Omega N_{n1} N_{m1} \mathrm{d}\alpha\mathrm{d}\beta \int_A F_{u_z s} F_{u_z \tau} \frac{H_\beta}{H_\alpha} \mathrm{d}z \\
& + C_{12} \frac{1}{R_\alpha R_\beta} N_j^{n2} N_i^{m1} \int_\Omega N_{n2} N_{m1} \mathrm{d}\alpha\mathrm{d}\beta \int_A F_{u_z s} F_{u_z \tau} \mathrm{d}z \\
& + C_{12} \frac{1}{R_\alpha R_\beta} N_j^{n1} N_i^{m2} \int_\Omega N_{n1} N_{m2} \mathrm{d}\alpha\mathrm{d}\beta \int_A F_{u_z s} F_{u_z \tau} \mathrm{d}z \\
& + C_{13} \frac{1}{R_\alpha} N_i^{m1} \int_\Omega N_j N_{m1} \mathrm{d}\alpha\mathrm{d}\beta \int_A F_{u_z s,z} F_{u_z \tau} H_\beta \mathrm{d}z \\
& + C_{22} \frac{1}{R_\beta^2} N_j^{n2} N_i^{m2} \int_\Omega N_{n2} N_{m2} \mathrm{d}\alpha\mathrm{d}\beta \int_A F_{u_z s} F_{u_z \tau} \frac{H_\alpha}{H_\beta} \mathrm{d}z \\
& + C_{23} \frac{1}{R_\beta} N_i^{m2} \int_\Omega N_j N_{m2} \mathrm{d}\alpha\mathrm{d}\beta \int_A F_{u_z s,z} F_{u_z \tau} H_\alpha \mathrm{d}z \\
& + C_{33} \int_\Omega N_j N_i \mathrm{d}\alpha\mathrm{d}\beta \int_A F_{u_z s,z} F_{u_z \tau,z} H_\alpha H_\beta \mathrm{d}z \\
& + C_{44} N_{j,\beta}^{n2} N_{i,\beta}^{m2} \int_\Omega N_{n2} N_{m2} \mathrm{d}\alpha\mathrm{d}\beta \int_A F_{u_z s} F_{u_z \tau} \frac{H_\alpha}{H_\beta} \mathrm{d}z \\
& + C_{55} N_{j,\alpha}^{n1} N_{i,\alpha}^{m1} \int_\Omega N_{n1} N_{m1} \mathrm{d}\alpha\mathrm{d}\beta \int_A F_{u_z s} F_{u_z \tau} \frac{H_\beta}{H_\alpha} \mathrm{d}z
\end{aligned} \tag{53}
$$

Data availability

Data will be made available on request.

References

Argyris, J.H., 1965. Matrix analysis of three-dimensional elastic media - small and large displacements. AIAA J. 3 (1), 45–51.

Argyris, J.H., 1966. Matrix displacement analysis of plates and shells, prolegomena to a general theory, part I. Ingeniur- Arch. 35, 102–142.

Bathe, K.J., 1996. Finite Element Procedure. Prentice hall, Upper Saddle River, New Jersey, USA.

Bathe, K.-J., Dvorkin, E.N., 1986. A formulation of general shell elements—the use of mixed interpolation of tensorial components. Internat. J. Numer. Methods Engrg. 22, 697–722.

Berdichevsky, V.L., 2010. An asymptotic theory of sandwich plates. Internat. J. Engrg. Sci. 48 (3), 383–404.

Bhimaraddi, A., 1984. A higher order theory for free vibration analysis of circular cylindrical shells. Int. J. Solids Struct. 20 (7), 623–630.

Blanco, P.J., Feijóo, R.A., Urquiza, S.A., 2008. A variational approach for coupling kinematically incompatible structural models. Comput. Methods Appl. Mech. Engrg. 197 (17), 1577–1602.

Bucalem, M.L., Bathe, K.J., 1993. Higher-order MITC general shell elements. Internat. J. Numer. Methods Engrg. 36 (21), 3729–3754.
Carrera, E., 1999a. Multilayered shell theories accounting for layerwise mixed description, part 1: Governing equations. AIAA J. 37 (9), 1107–1116.
Carrera, E., 1999b. Multilayered shell theories accounting for layerwise mixed description, part 2: Numerical evaluations. AIAA J. 37 (9), 1117–1124.
Carrera, E., 2001. Developments, ideas, and evaluations based upon Reissner's mixed variational theorem in the modeling of multilayered plates and shells. Appl. Mech. Rev. 54 (4), 301–329.
Carrera, E., 2003. Theories and finite elements for multilayered plates and shells: A unified compact formulation with numerical assessment and benchmarking. Arch. Comput. Methods Eng. 10, 215–296.
Carrera, E., Cinefra, M., Lamberti, A., Petrolo, M., 2015. Results on best theories for metallic and laminated shells including layer-wise models. Compos. Struct. 126, 285–298.
Carrera, E., Cinefra, M., Petrolo, M., Zappino, E., 2014. Finite Element Analysis of Structures Through Unified Formulation. John Wiley & Sons.
Carrera, E., Miglioretti, F., Petrolo, M., 2011. Accuracy of refined finite elements for laminated plate analysis. Compos. Struct. 93 (5), 1311–1327.
Carrera, E., Pagani, A., Scano, D., 2024a. Legendre-based node-dependent kinematics shell models for the global–local analysis of homogeneous and layered structures. Int. J. Solids Struct. 289, 112630.
Carrera, E., Petrolo, M., 2010a. Guidelines and recommendations to construct theories for metallic and composite plates. AIAA J. 48 (12), 2852–2866.
Carrera, E., Petrolo, M., 2010b. On the effectiveness of higher-order terms in refined beam theories. J. Appl. Mech. 78 (2).
Carrera, E., Scano, D., 2024. Complete variable kinematic CUF-based multilayered shell elements. In: 16th World Congress on Computational Mechanics and 4th Pan American Congress on Computational Mechanics.
Carrera, E., Scano, D., Zappino, E., 2024b. One-dimensional Finite Elements with Arbitrary Cross-Sectional Displacement Fields. (Under review).
Carrera, E., Scano, D., Zappino, E., 2025. Plate finite elements with arbitrary displacement fields along the thickness. Finite Elem. Anal. Des. 244, 104296.
Carrera, E., Valvano, S., Kulikov, M., 2018. Electro-mechanical analysis of composite and sandwich multilayered structures by shell elements with node-dependent kinematics. Int. J. Smart Nano Mater. 9 (1), 1–33.
Cicala, P., 1959. Sulla teoria elastica della parete sottile. Giornala Del Genio Civ. fascicoli 4, 6 e 9.
Cicala, P., 1965. Systematic Approximation Approach to Linear Shell Theory. Levrotto e Bella, Turin, Italy.
Cinefra, M., 2022. Formulation of 3D finite elements using curvilinear coordinates. Mech. Adv. Mater. Struct. 29 (6), 879–888.
Cinefra, M., Carrera, E., 2013. Shell finite elements with different through-the-thickness kinematics for the linear analysis of cylindrical multilayered structures. Internat. J. Numer. Methods Engrg. 93 (2), 160–182.
Cinefra, M., Valvano, S., Carrera, E., 2016. Thermal stress analysis of laminated structures by a variable kinematic MITC9 shell element. J. Therm. Stresses 39 (2), 121–141.
Cofer, W.F., Will, K.M., 1991. A three-dimensional, shell-solid transition element for general nonlinear analysis. Comput. Struct. 38 (4), 449–462.
Dávila, C.G., 1994. Solid-to-shell transition elements for the computation of interlaminar stresses. Comput. Syst. Eng. 5 (2), 193–202.
Demasi, L., 2008. ∞^3 hierarchy plate theories for thick and thin composite plates: The generalized unified formulation. Compos. Struct. 84 (3), 256–270.
Demasi, L., 2013. Partially layer wise advanced Zig Zag and HSDT models based on the generalized unified formulation. Eng. Struct. 53, 63–91.
Flügge, W., 1934. Statik und Dynamic der Schalen. Springer-Verlag.
Gol'denveizer, A.L., 1961. Theory of Elastic Thin Shells. Pergamon Press, Oxford, United Kingdom.
Hildebrand, F.B., Reissner, E., Thomas, G.B., 1940. Notes on the foundations of the theory of small displacement of orthotropic shells. NACA TN- 1833.
Khare, R.K., Kant, T., Garg, A.K., 2004. Free vibration of composite and sandwich laminates with a higher-order facet shell element. Compos. Struct. 65 (3), 405–418.
Kirchhoff, G., 1850. Über das gleichgewicht und die bewegung einer elastischen scheibe. J. Für Die Reine Und Angew. MAthematik 40, 51–88.
Lee, C.-Y., Hodges, D.H., 2009. Asymptotic construction of a dynamic shell theory: Finite-element-based approach. Thin-Walled Struct. 47 (3), 256–270.
Liao, C.L., Reddy, J.N., Engelstad, S.P., 1988. A solid-shell transition element for geometrically non-linear analysis of laminated composite structures. Internat. J. Numer. Methods Engrg. 26 (8), 1843–1854.
Lindberg, G.M., Olson, M.D., Cowper, G.R., 1969. New developments in the finite element analysis of shells. Q. Bull. Div. Mech. Eng. Natl. Aeronaut. Establ. 4, 1–38.
Mindlin, R.D., 1951. Influence of rotary inertia and shear on flexural motions of isotropic, elastic plates. J. Appl. Mechanics- Trans. Asme 18, 31–38.
Naghdi, P.M., 1956. A survey of recet progress in the theory of elastic shells. Appl. Mech. Rev. 9, 365–368.
Noor, A.K., 1986. Global-local methodologies and their application to nonlinear analysis. Finite Elem. Anal. Des. 2 (4), 333–346.
Noor, A.K., Burton, W.S., 1990. Assessment of computational models for multilayered composite shells. Appl. Mech. Rev. 43, 67–97.
Pagani, A., Carrera, E., Scano, D., Augello, R., 2023. Finite elements based on Jacobi shape functions for the analysis of beams, plates and shells. Internat. J. Numer. Methods Engrg. 124 (20), 4490–4519.
Palazotto, A.N., Dennis, S.T., 1992. Nonlinear analysis of shell structures. AIAA Series.
Petrolo, M., Augello, R., Carrera, E., Scano, D., Pagani, A., 2023. Evaluation of transverse shear stresses in layered beams/plates/shells via stress recovery accounting for various CUF-based theories. Compos. Struct. 307, 116625.
Petrolo, M., Carrera, E., 2019. Best theory diagrams for multilayered structures via shell finite elements. Adv. Model. Simul. Eng. Sci. 6 (4), 1–23.
Petrolo, M., Lamberti, A., 2016. Axiomatic/asymptotic analysis of refined layer-wise theories for composite and sandwich plates. Mech. Adv. Mater. Struct. 23 (1), 28–42.
Petrolo, M., Lamberti, A., Miglioretti, F., 2016. Best theory diagram for metallic and laminated composite plates. Mech. Adv. Mater. Struct. 23 (9), 1114–1130.
Pryor, C.W., Baeker, R.M., 1971. A finite-element analysis including transverse shear effects for applications to laminated plates. AIAA J. 9 (5), 912–917.
Reddy, J.N., 1997. Mechanics of Laminated Composite Plates and Shells: Theory and Analysis. CRC Press, New York, USA.
Reddy, J.N., Liu, C., 1985. A higher-order shear deformation theory of laminated elastic shells. Internat. J. Engrg. Sci. 23 (3), 319–330.
Reissner, E., 1945. The effect of transverse shear deformation on the bending of elastic plates. J. Appl. Mech. 12, 69–77.
Reissner, E., 1975. On transverse bending of plates, including the effect of transverse shear deformation. Int. J. Solids Struct. 11 (5), 569–573.
Surana, K.S., 1980. Transition finite elements for three-dimensional stress analysis. Internat. J. Numer. Methods Engrg. 15 (7), 991–1020.
Surana, K.S., 1982. Geometrically non-linear formulation for the three dimensional solid-shell transition finite elements. Comput. Struct. 15 (5), 549–566.
Thakur, S.N., Ray, C., Chakraborty, S., 2018. Response sensitivity analysis of laminated composite shells based on higher-order shear deformation theory. Arch. Appl. Mech. 88 (8), 1429–1459.
Washizu, K., 1968. Variational Methods in Elasticity and Plasticity. Pergamon, Oxford, United Kingdom.
Wu, B., Pagani, A., Chen, W.Q., Carrera, E., 2021. Geometrically nonlinear refined shell theories by carrera unified formulation. Mech. Adv. Mater. Struct. 28 (16), 1721–1741.
Yu, W., Hodges, D.H., Volovoi, V.V., 2002. Asymptotic generalization of Reissner–Mindlin theory: accurate three-dimensional recovery for composite shells. Comput. Methods Appl. Mech. Engrg. 191 (44), 5087–5109.
Zappino, E., Carrera, E., 2018. Multidimensional model for the stress analysis of reinforced shell structures. AIAA J. 56 (4), 1647–1661.